NACA

RESEARCH MEMORANDUM

AERODYNAMIC CHARACTERISTICS AT MACH NUMBERS FROM 2.5

TO 3.5 OF A CANARD BOMBER CONFIGURATION DESIGNED

FOR SUPERSONIC CRUISE FLIGHT

By Melvin M. Carmel, Thomas C. Kelly,
and Donald T. Gregory

Langley Aeronautical Laboratory
Langley Field, Va.

NATIONAL ADVISORY COMMITTEE
FOR AERONAUTICS
WASHINGTON
September 10, 1958

NATIONAL ADVISORY COMMITTEE FOR AERONAUTICS

RESEARCH MEMORANDUM

AERODYNAMIC CHARACTERISTICS AT MACH NUMBERS FROM 2.5

TO 3.5 OF A CANARD BOMBER CONFIGURATION DESIGNED

FOR SUPERSONIC CRUISE FLIGHT*

By Melvin M. Carmel, Thomas C. Kelly,
and Donald T. Gregory

SUMMARY

Results have been obtained from an investigation in the Langley
Unitary Plan wind tunnel at Mach numbers from 2.5 to 3.5 of a canard-
type configuration designed for supersonic cruise flight. Tests extended
over an angle-of-attack range from about -4° to 11° and an angle-of-
sideslip range from -4° to 6°.

For the present tests, the results indicate that forebody deflection
was an efficient means of providing a sizable positive pitching-moment
shift with little or no increase in drag. The test configuration had a
trimmed lift-drag ratio of approximately 6.0 at Mach numbers near 3.0 and
at a Reynolds number of 2.52×10^6. The configuration was both longitudi-
nally and directionally stable. The lift-drag ratios are believed to be
somewhat low inasmuch as the models used for the present tests had large-
grain-size transition strips fixed to the various surfaces and these strips
added wave drag. Also, the model boundary-layer diverter is oversized
with respect to a full-scale configuration and therefore contributes
additional drag.

INTRODUCTION

The preliminary investigation of the canard bomber configuration of
reference 1 showed that cruising flight at Mach numbers near 3 is feas-
ible. The configuration tested, however, was deficient in directional
stability at low angles of attack. In addition, it had a negative zero-
lift pitching moment that required excessive canard deflection for trim

---

*Title, Confidential.

even at the relatively low static margin of about $0.04\bar{c}$; thus, a substantial increase in the trim drag and decreases in $(L/D)_{max}$ result. The maximum lift-drag ratio was probably further reduced by the increased drag of the unporting of the canard at the required deflections. The deficiencies noted are superficial rather than fundamental and the present investigation was conducted to show how they might be corrected by relatively simple modifications. The results of reference 2 have shown that deflecting the forebody of a fuselage can produce substantial changes in the zero-lift pitching moment without appreciably increasing the drag. The forebody of the canard bomber configuration was therefore deflected upward approximately 3° and flattened somewhat to provide a positive zero-lift pitching-moment increment. In order to provide greater directional stability at low angles of attack, the ventral fins of the model were also enlarged. The tests were made for a Mach number range from 2.5 to 3.5, and angle-of-attack range from -4° to 11°, and an angle-of-sideslip range from about -4° to 6°. Included are the effects of a variation in Reynolds number and transition grain size. Results are presented with only a brief analysis in order to expedite publication.

SYMBOLS

The aerodynamic force and moment data are referred to the stability axes for the longitudinal data and the body axes for the lateral data (figs. 1 and 2) with the origin at the center of gravity $(0.214\bar{c})$. Symbols used are defined as follows:

b   wing span, in.

$\bar{c}$ wing mean aerodynamic chord, in.

$C_D{'}$ drag coefficient, $F_D{'}/qS$

$C_{D,b}{'}$ base drag coefficient, $\dfrac{\text{Base drag}}{qS}$

$C_{D,c}{'}$ chamber drag coefficient, $\dfrac{\text{Chamber drag}}{qS}$

$C_{D,i}{'}$ internal duct drag coefficient, $\dfrac{\text{Internal duct drag}}{qS}$

C_L lift coefficient, F_L/qS

C_l rolling-moment coefficient, $\dfrac{\text{Rolling moment}}{qSb}$

C_m pitching-moment coefficient, $\dfrac{\text{Pitching moment}}{qS\bar{c}}$

C_n yawing-moment coefficient, $\dfrac{\text{Yawing moment}}{qSb}$

C_Y side-force coefficient, F_Y/qS

F_D drag force, lb

F_L lift force, lb

F_Y side force, lb

$(L/D)_{max}$ maximum lift-drag ratio

M free-stream Mach number

q free-stream dynamic pressure, lb/sq ft

R Reynolds number based on $\bar{c}$

S wing area, sq ft

α angle of attack of bottom surface of wing, deg

β angle of sideslip of fuselage center line, deg

δ_c canard angle relative to wing lower surface (positive direction, trailing edge down), deg

δ_e elevon angle relative to wing lower surface (positive direction, trailing edge down), deg

δ_n angle of nose center line relative to wing lower surface (positive direction, nose up), deg

$C_{L_\alpha} = \dfrac{\partial C_L}{\partial \alpha}$ per degree

$C_{l_\beta} = \dfrac{\partial C_l}{\partial \beta}$ per degree

$C_{m_{C_L}} = \dfrac{\partial C_m}{\partial C_L}$

$$C_{n_\beta} = \frac{\partial C_n}{\partial \beta} \quad \text{per degree}$$

$$C_{Y_\beta} = \frac{\partial C_Y}{\partial \beta} \quad \text{per degree}$$

$$C_{m_{\delta_c}} = \frac{\partial C_m}{\partial \delta_c} \quad \text{per degree}$$

APPARATUS AND TESTS

Tunnel

Tests were conducted in the high Mach number test section of the Langley Unitary Plan wind tunnel, which is a variable-pressure continuous-flow tunnel. The nozzle leading to the test section is of the asymmetric sliding-block type, which permits a continuous variation in test section Mach number from about 2.3 to 4.7.

Model

A three-view drawing and design dimensions of the basic model tested are shown in figure 3(a) and table I, respectively. The model wing had a delta plan form with the outer 42 percent of the semispan removed, 62° sweepback of the leading edge, an aspect ratio of 0.904, a taper ratio of 0.437, and 2.5 percent-thick half double-wedge airfoil sections with maximum thickness at 70 percent chord. This configuration is essentially the same as that reported in reference 1. It differs only in forebody shape and in the ventral fins. For purposes of clarity, the model components as tested in reference 1 will hereinafter be referred to as "original" and the redesigned components of the present tests will be designated as "modified."

The forebody configurations are shown in figure 3(b). The modified forebody has a plan form identical to that of the original forebody but is wedge shaped in side elevation. (See figs. 3(a) and 3(b).) This results in a considerable flattening of the cross sections over the forward body regions. In addition, the modified forebody was made slab sided in the vicinity of the canard in order to prevent the canard from unporting between incidence angles of $\pm 5^\circ$ (measured relative to the forebody center line). Provision was made to test the modified forebody configuration at angles of incidence (relative to the wing lower surface) of 0° and 2.9°. With the forebody at an angle of 2.9° the upper body

line became straight from the model nose to a point approximately 25 inches back of the model nose. (See fig. 3(a)). The point selected for rotation of the forebody was taken as the 20-inch model station (canard trailing-edge station).

The canard control surface, identical to that of reference 1, has a delta plan form with provision made to test the canard at angles of deflection (relative to the wing lower surface) of 0°, 2.9^{o}, and 7.9^{o}. For these tests, the hinge line of the canard was placed at 57 percent of the canard-body juncture chord. (The canard hinge line for the tests of reference 1 was located at 67 percent of the canard-body juncture chord.)

The vertical-fin surfaces employed in the present tests are designated as original ventral fins, modified ventral fins, and upper-surface vertical fins and are shown in figure 3(c). The upper-surface vertical fins were tested both at the wing tips and at the 0.3b/2 station.

Elevons, mounted at the rear, outboard portions of the wing, were designed to permit testing at deflections of 0° and $\pm10^{o}$. Other model characteristics are identical to those of the model of reference 1. Model photographs are presented in figure 4.

Test Conditions and Procedure

Most of the tests were conducted at Mach numbers of 2.5, 3.0, and 3.5 and at stagnation pressures that were varied in order to provide a constant test Reynolds number of 2.52×10^{6} based on the wing mean aerodynamic chord. The stagnation temperature was 150° F. The dewpoint, measured at stagnation pressure, was maintained below -30° F in order to assure negligible condensation effects. The angle-of-attack range varied from approximately -4° to 11° and the angle-of-sideslip range varied from about -4° to 6°. Characteristics of the model in sideslip were obtained at angles of attack of approximately 0°, 4°, and 10° at a Mach number of 3.0.

Most of the tests were conducted with transition fixed at 5 percent of the wing, canard, and vertical surface chords, and at a location 1 inch back of the model nose. These transition strips were composed of 0.031-inch grains of sand spaced approximately 0.1 inch apart. (See fig. 4.) In addition, brief tests were conducted with transition strips of a smaller grain size and with natural boundary-layer transition. The smaller strips were about 0.1 inch wide and were composed of No. 60 carborundum grains (average size, 0.012 inch) set in a plastic adhesive.

For the three model surface conditions and the three model forebody configurations, tunnel stagnation pressures were varied in order to

determine the effect of a variation in Reynolds number on the model drag characteristics. Resulting Reynolds numbers varied from 2.52×10^6 to about 15.5×10^6.

Measurements

Aerodynamic forces and moments were determined by means of a six-component electrical strain-gage balance housed within the engine package. The balance, in turn, was rigidly fastened to a sting support system and provision was made to detect any fouling between the model and sting support system.

Balance chamber pressure was measured with a single static orifice located in the vicinity of the strain-gage balance. Base-pressure measurements were made on one side of the model base only by using two multi-orifice tubes which encircled approximately equal segments of the model base. (See fig. 4(b).) Pressures from these tubes were averaged. Duct exit pressures were determined on one side of the model base by means of four-tube total-pressure rakes placed in each of the three circular exits. Each rake was manifolded to a single tube in order to provide an average total pressure for the duct exit. A check to determine the existence of sonic flow at the duct exit was made by means of a static-pressure measurement at one of the duct exits. (The duct exit was sized to obtain sonic flow and thereby facilitate computations of internal drag.) Schlieren photographs of each of the model forebody configurations were taken at various attitudes at a Mach number of 3.0. (See fig. 5.)

Corrections

Calibration of the tunnel test section has indicated that model buoyancy effects are negligible. Corrections to the indicated model angle of attack have been made for both tunnel air-flow misalinement and deflection of model and sting support due to load.

The drag data presented herein have been adjusted to correspond to zero balance chamber and base drag coefficients. In addition, the internal or duct drag has been subtracted from the adjusted drag values and the drag coefficients presented in this paper represent the net external drag of the model. The magnitude of these drag adjustments may be found in figure 6.

Accuracy

Based upon balance calibration and repeatability of data, it is estimated that the various measured quantities are accurate within the following limits at low lift coefficients:

C_L . . . . ± 0.006

C_D' . . . . ± 0.001

$C_{D,b}'$ . . . . ± 0.0002

$C_{D,c}'$ . . . . ± 0.0002

$C_{D,i}'$ . . . . ± 0.0002

C_m . . . . ± 0.001

C_l . . . . ± 0.0002

C_n . . . . ± 0.0005

C_Y . . . . ± 0.002

α, deg . . . . ± 0.15

β, deg . . . . ± 0.10

The maximum deviation of the local Mach number from the free-stream values given is ± 0.015.

RESULTS AND DISCUSSION

Schlieren photographs of the various forebody configurations are presented in figure 5 and experimental results are presented in figures 6 to 21.

Effect of Forebody Configuration

Longitudinal characteristics.- Comparison of the drag and longitudinal stability characteristics at a Mach number of 3.00 for the original and the undeflected modified forebody configurations indicates only slight variations in the aerodynamic characteristics resulting from a change in forebody shape. Increasing the deflection of the modified forebody from $0°$ to $2.9°$ has little effect on the lift and drag characteristics (fig. 7) but does provide a positive increment in pitching-moment coefficient at $C_L = 0$ of approximately 0.008. Increasing the canard angle from $0°$ to $2.9°$ with the forebody deflected up $2.9°$ leads to a further gain in C_m at $C_L = 0$ of approximately 0.008; thus, for equal deflection angles, the forebody and the canard are equally effective near $C_L = 0$

in producing trim changes for the configuration. The results presented in figure 7 indicate that the configuration having 2.9° ($\delta_c = 2.9^\circ$) of forebody deflection trims at lift coefficients near those for $(L/D)_{max}$ with little or no penalty in drag, whereas the undeflected forebody configuration would have an increased drag due to trimming. (See ref. 1.)

Lateral characteristics.- Results presented in figures 8 or 9 show that at a Mach number of 3.00 an increase in forebody and canard deflection from 0° to 2.9° is accompanied by an increase in positive dihedral effect at angles of attack near 0° and 4° but has only a slight effect at angles of attack near 10°. The change in dihedral effect is believed to be primarily due to canard deflection. Forebody and canard deflection has only slight effects on C_{n_β} and C_{Y_β}. (See fig. 9.)

Effects of Reynolds Number and Transition

The variations of minimum drag coefficient with Reynolds number for the three forebody configurations are shown in figure 10 for a Mach number of 3.00. These curves show the expected decrease in minimum drag coefficient with an increase in test Reynolds number, the decrease being of the same order of magnitude as that calculated on the basis of a reduction in skin-friction drag coefficient accompanying an increase in Reynolds number.

It may also be noted that, on this somewhat expanded drag scale, the modified forebody configurations are seen to have slightly less drag than the original forebody configuration. Although the differences noted are close to the accuracy of measurement at Reynolds numbers near 2.52×10^6, test accuracy increases with an increase in Reynolds number, and the differences noted at the higher Reynolds numbers may be considered to be realistic. Therefore, deflecting the modified forebody upward 2.9° not only allows the configuration to trim at lift coefficients near those for $(L/D)_{max}$ as noted in the previous section but also provides a higher $(L/D)_{max}$ because of the lowered drag level resulting from the forebody modification.

Figure 11 shows, as would be expected, that fixing transition on the 2.9° deflected forebody configuration has little or no effect on the lift and pitch characteristics but does result in slight increases in drag, the highest drag level occurring for the model having the largest transition grain size.

Variations of minimum drag coefficient with Reynolds number (fig. 12) show the curves for the 0.031-inch and 0.012-inch-grain-size strips and

for the model with natural transition to be approximately parallel throughout the test Reynolds number range. It may be assumed from these curves that the model boundary layer was turbulent for the natural transition case and that the addition of transition particles added only wave drag. It should be noted that the following sections of this paper present results obtained from models having the 0.031-inch-grain-size transition strips; therefore, the general drag levels are increased slightly and the $(L/D)_{max}$ values presented for these configurations are believed to be somewhat low.

Effect of Canard and Elevon Deflection

Canard characteristics.- The effects of canard deflection on the basic longitudinal aerodynamic characteristics for the deflected forebody configuration are shown in figure 13. Variations with Mach number of lift and pitching-moment curve slopes (fig. 14) indicate that canard deflection has little effect on these parameters. As would be expected, addition of the canard results in an increase in lift-curve slope and a substantial decrease in stability level. The canard effectiveness parameter, shown in figure 15, exhibits the usual reduction in canard effectiveness with increase in Mach number; this condition is a result of the reduction in canard lift-curve slope which accompanies an increase in Mach number.

Maximum lift-drag ratios for the configurations (fig. 14) indicate that no penalty results from increasing canard incidence from 0° to 2.9^O. Further increases in canard angle to 7.9^O are accompanied by a decrease in $(L/D)_{max}$ amounting to about 10 percent at a Mach number of 3.00. Examination of the curves presented in figure 13 indicates that a canard incidence angle of 2.9^O trims the deflected forebody configuration at a lift coefficient higher than that for $(L/D)_{max}$. Therefore, maximum trimmed lift-drag ratios for this configuration would be as high as the untrimmed $(L/D)_{max}$ values presented for canard incidence angles of 0° and 2.9^O.

Elevon characteristics.- The effects of elevon deflection on the aerodynamic characteristics in pitch are shown for a Mach number of 3.00 in figure 16. These results indicate that a positive elevon deflection of 10° causes an increase in lift coefficient at constant angle of attack amounting to about 0.01, an increase in minimum drag coefficient level of about 0.0020, and a decrease in pitching-moment coefficient (at constant C_L) of about 0.008. It is interesting to note that the variation in pitching-moment increment obtained with 10° of elevon deflection is approximately equal to that obtained by varying the canard incidence angle from 0° to 2.9^O (fig. 13) although opposite in direction.

Comparison of the drag results for the elevon and canard deflections, however, indicates that the pitching-moment shift is obtained with the canard control with no measurable attendant increase in drag, whereas the shift in pitching moment with elevon deflection is accompanied by an increase in drag and a corresponding reduction in $(L/D)_{max}$.

Differential elevon deflection causes little or no variation in the lift and pitch characteristics when compared with the configuration having no elevon deflection and causes an increase in drag approximately equal to that caused by the positive elevon deflection.

The effects of differential elevon deflection on the aerodynamic characteristics in sideslip (fig. 17) indicate that at a Mach number of 3.00 C_{n_β}, C_{l_β}, and C_{Y_β} are only slightly affected by elevon deflection. Differential deflection does, however, increase C_l by about 0.004 and decreases C_n by 0.001 (adverse yawing moment) at angles of attack of $0°$ and $4°$. These effects become somewhat larger as the angle of attack is increased to $10°$ (fig. 17).

Effect of Vertical Surfaces

Longitudinal characteristics.- The effects of ventral and vertical fins on the basic aerodynamic characteristics in pitch are shown in figure 18.

Lift and pitching-moment curve slopes for the various vertical sur-face configurations, shown in figure 19, indicate two general trends. The configurations having ventral fins exhibit a slight increase in both lift-curve slope and in stability level when compared with the configura-tions having upper-surface fins or no fins. It should be noted here that the center-of-gravity location used for the present tests, which was at the approximate model center of volume, was selected to give a value of $\partial C_m / \partial C_L$ of about -0.05 at Mach numbers near 3.00 for the configuration having original ventral fins. Unpublished data indicate that this center-of-gravity location would lead to longitudinal insta-bility at subsonic Mach numbers. As noted in reference 1, some means must be provided in order to obtain a stable subsonic configuration.

Maximum lift-drag ratios for the various configurations at a Mach number of 3.00 and a Reynolds number of 2.5×10^6 (fig. 19) range from 6.1 for the original ventral fin configuration to 5.8 for the modified ventral fin configuration. It is felt that these results should not be used to select a "most desirable" fin shape or location inasmuch as variations in C_L or C_D equal to the stated test accuracies

$\left(0.006 \text{ for } C_L \text{ and } 0.0010 \text{ for } C_D\right)$ would cause variations in $\left(L/D\right)_{max}$ equal to those shown above.

Lateral characteristics.- The effects of ventral and vertical fins on the aerodynamic characteristics in sideslip are presented in figures 20 and 21. The results of figure 21 show that the model with the original ventral fins is directionally unstable at angles of attack near 0°. The stability increases with an increase in angle of attack, however, and the configuration becomes stable at angles of attack near 4°. Enlargement of the ventral fins adds a relatively constant positive increment in C_{n_β} throughout the test angle-of-attack range, and the modified ventral fin configuration is stable at all positive angles of attack tested.

With the ventral fins removed, installation of upper-surface vertical fins at either the 0.3b/2 station or at the wing tips provides configurations that are directionally stable at angles of attack near 0°. With the vertical fins at the 0.3b/2 station, the directional stability decreases immediately as the angle of attack is increased from 0°, and the configuration becomes unstable at angles of attack near 4°. This deterioration in directional stability is delayed when the vertical fins are placed at the wing tips and the reduction in C_{n_β} does not begin until angles of attack of about 4° are reached. This latter configuration, however, still maintains a slight degree of positive directional stability at the highest test angle of attack.

All configurations exhibit positive effective dihedral, the dihedral effect being increased for the configurations having upper-surface vertical fins.

SUMMARY OF RESULTS

An investigation conducted at Mach numbers from 2.5 to 3.5 of a canard-type configuration designed for supersonic cruise flight have indicated the following results:

Forebody deflection was found to be an efficient means of providing a sizable positive pitching-moment shift with little or no increase in drag. It appears possible to obtain trimmed lift-drag ratios of approximately 6.0 at Mach numbers near 3.0 and at a Reynolds number of 2.52×10^6 for a canard-type configuration that is both longitudinally and directionally stable. It should be noted that these values may be somewhat low inasmuch as the models used for the present tests had large-grain-size transition strips fixed to the various surfaces

and these strips added some wave drag. In addition, as noted in NACA Research Memorandum L58B28, the model boundary-layer diverter is over- sized with respect to a full-scale configuration and therefore contrib- utes additional drag.

Langley Aeronautical Laboratory,
    National Advisory Committee for Aeronautics,
        Langley Field, Va., July 1, 1958.

REFERENCES

1. Kelly, Thomas C., Carmel, Melvin M., and Gregory, Donald T.: An Exploratory Investigation at Mach Numbers of 2.50 and 2.87 of a Canard Bomber-Type Configuration Designed for Supersonic Cruise Flight. NACA RM L58B28, 1958.

2. Spearman, M. Leroy, and Driver, Cornelius: Some Factors Affecting the Stability and Performance Characteristics of Canard Aircraft Configurations. NACA RM L58D16, 1958.

TABLE I.- MODEL DESIGN DIMENSIONS

Wing:
  Area, sq ft 4.183
  Span, in. 23.33
  Root chord, in. 36.00
  Tip chord, in. 15.73
  Aspect ratio 0.904
  Taper ratio 0.437
  Mean aerodynamic chord, in. 27.04
  Leading-edge sweep, deg 62
  Airfoil section . . . . Double wedge, flat lower surface
  Thickness ratio with $(t/c)_{max}$ at 0.7c 0.025

Canard:
  Area (total), sq ft 0.700
  Area (exposed) sq ft 0.370
  Span, in. 14.66
  Root chord, in. 13.75
  Tip chord, in. 0
  Aspect ratio 2.13
  Taper ratio 0
  Mean aerodynamic chord, in. 9.17
  Leading-edge sweep, deg 62
  Airfoil section . . . . Double wedge
  Thickness ratio with $(t/c)_{max}$ at 0.7c 0.025

Original ventral fins:
  Area, each, sq in. 26.08
  Airfoil section . . . . Single wedge

Modified ventral fins:
  Area, each, sq in. 41.95
  Airfoil section . . . . Modified double wedge

Vertical fins:
  Area, each, sq in. 30.08
  Height, in. 5.13
  Root chord, in. 9.03
  Tip chord, in. 2.70
  Aspect ratio 0.875
  Taper ratio 0.299
  Mean aerodynamic chord, in. 6.44
  Leading-edge sweep, deg 62
  Airfoil section . . . . Double wedge
  Thickness ratio with $(t/c)_{max}$ at 0.7c 0.025

Center-of-gravity location, percent overall length 62

Center-of-gravity, percent of mean aerodynamic chord 21.4
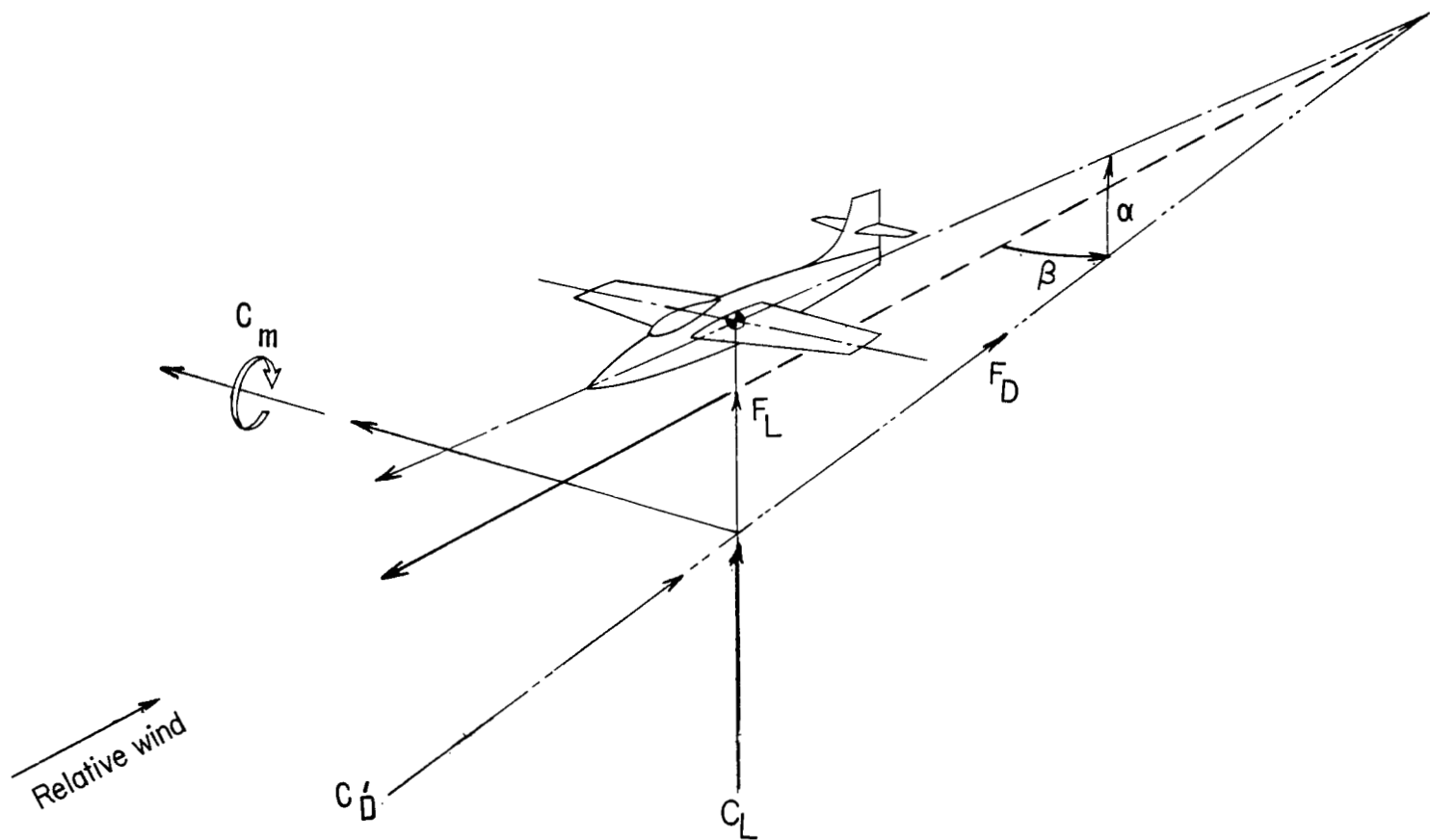
Figure 1.- Stability axes system.
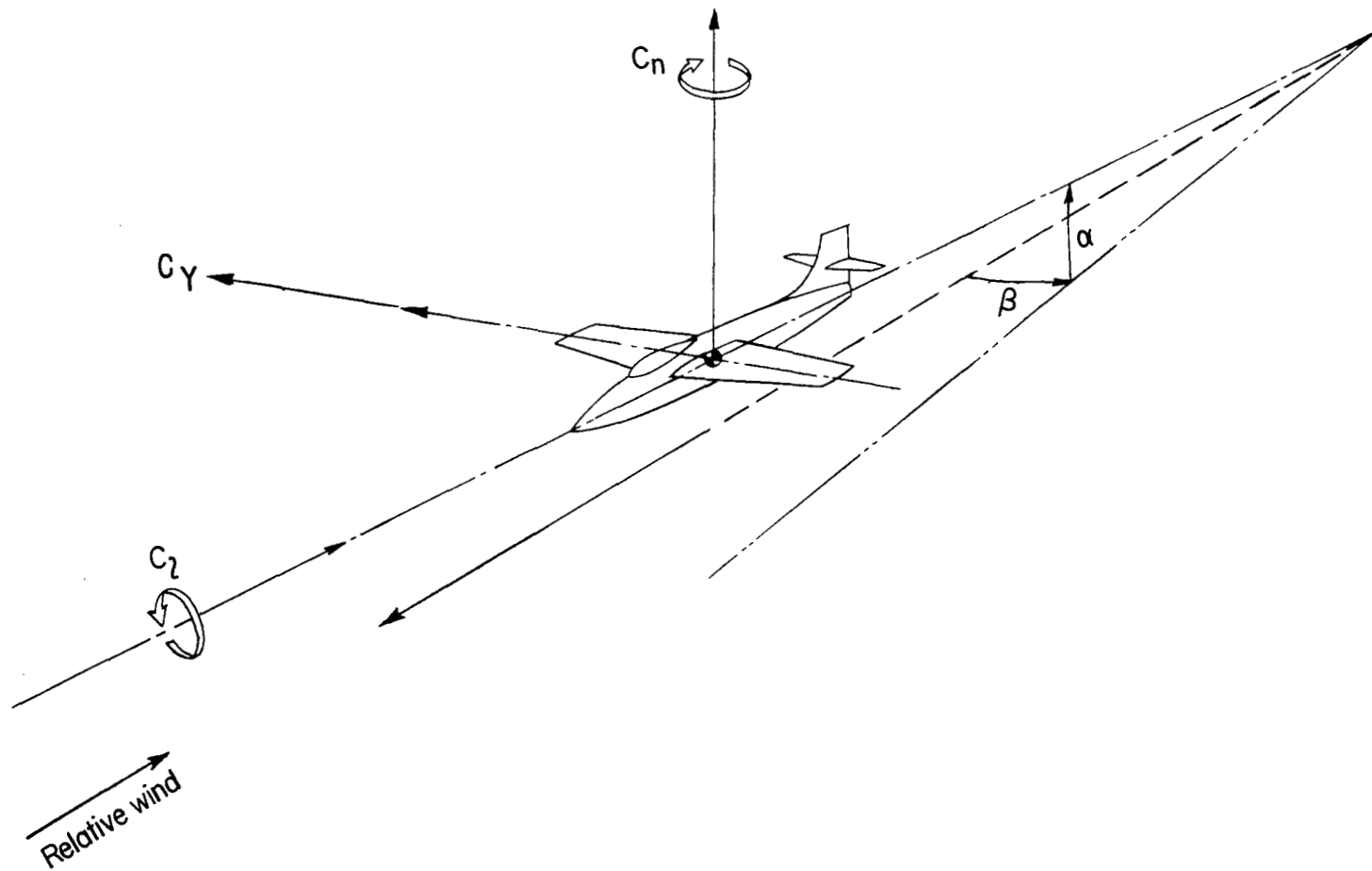
Figure 2.- Body axes system.

.7chord line

3.333

23.333

2.25

10.756

1.667

Canard
hinge line

62°

62°

.7 chord line

8.5°

8.5°

4.012

C.G.

5.063

5.67

7.33

6.760

c̄=27.04

10.00

10.00

24.997

15.733

2.5

41.350

65.167

2.006

3.62

A

B

C

A

B

C

1.583

.767

1.927

16.306

Section A-A   Section B-B   Section C-C

.897 diam
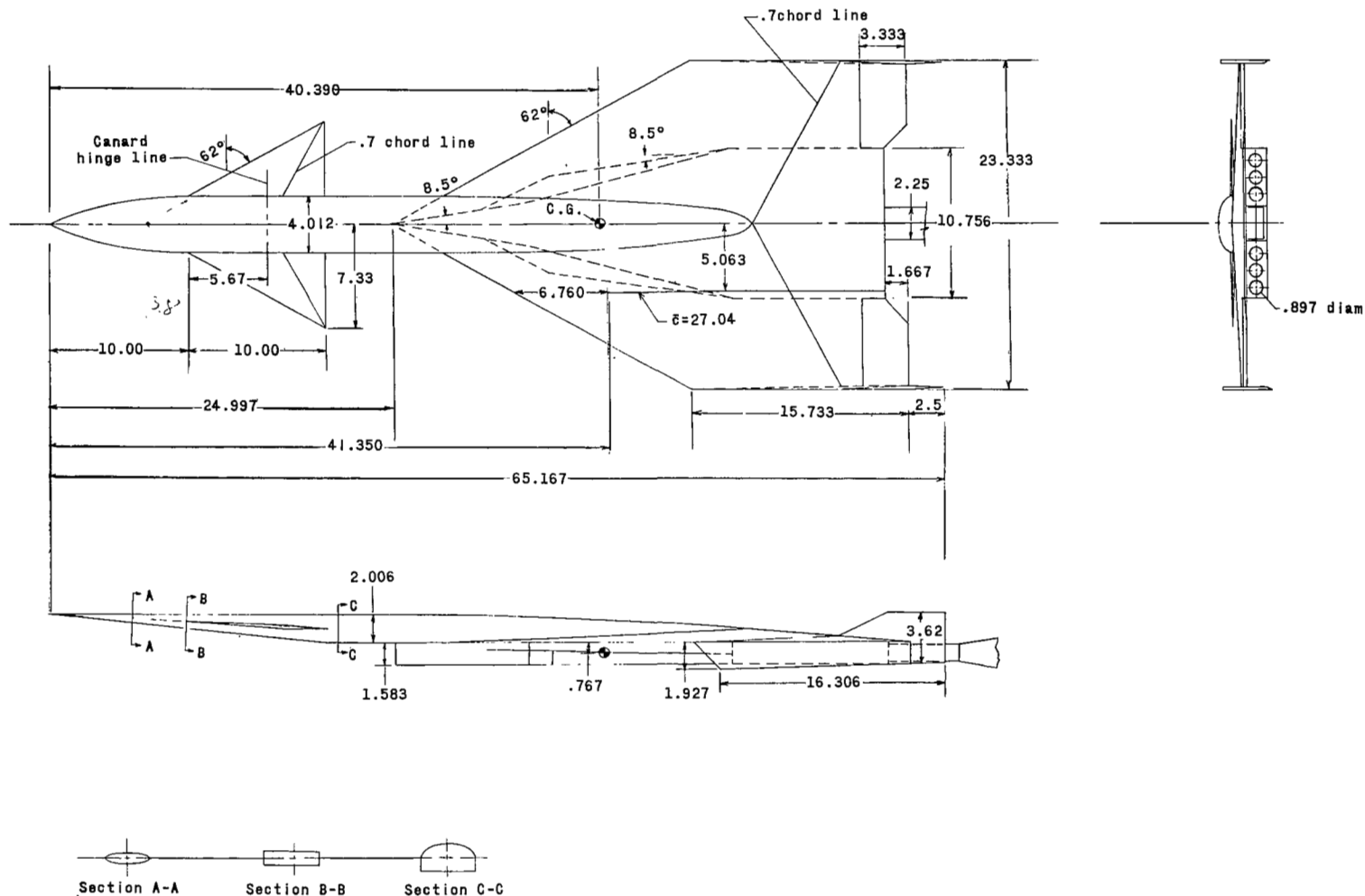
(a) Modified model.

Figure 3.- Model details. All dimensions are in inches unless otherwise noted.

Original forebody
Modified forebody at 0°
Modified forebody at 2.9°
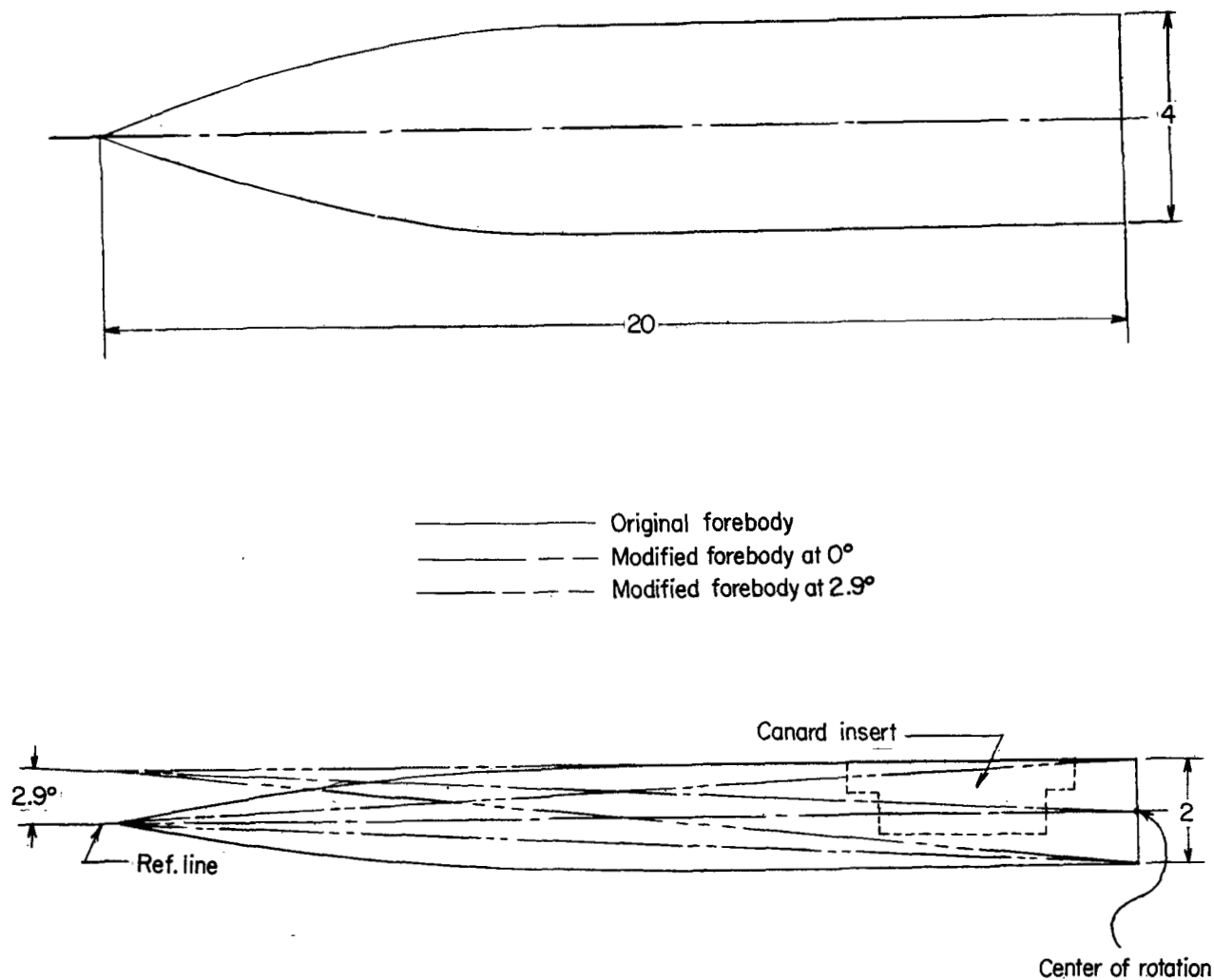
(b) Sketch of model forebodies.

Figure 3.- Continued.
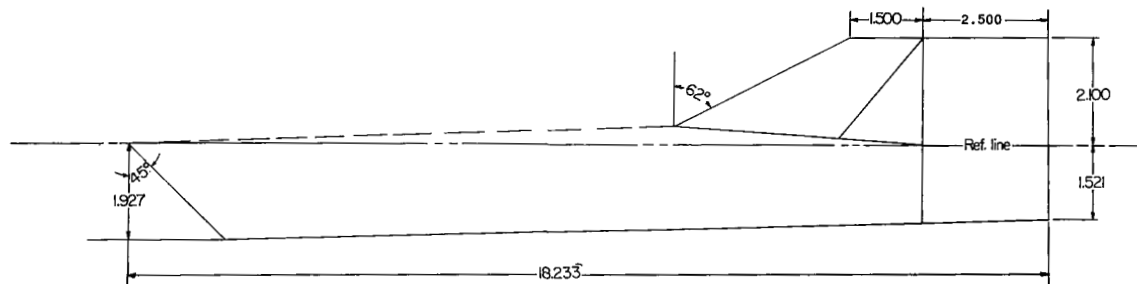
Modified ventral fin.
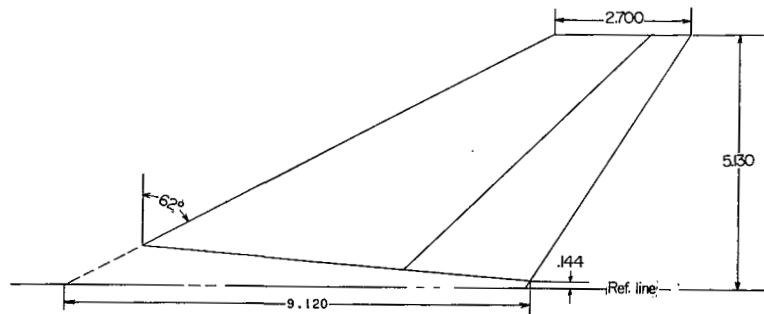
Upper-surface vertical fin.
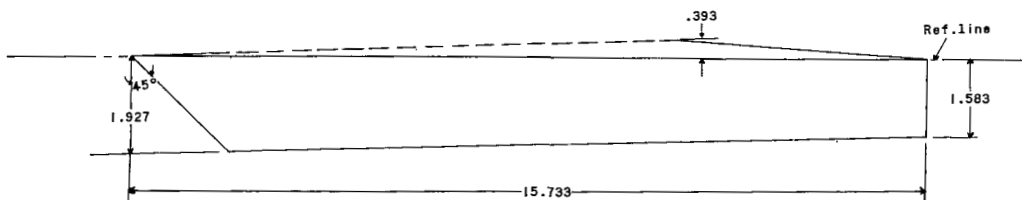
Original ventral fin.

(c) Sketch of vertical surfaces.

Figure 3.- Concluded.
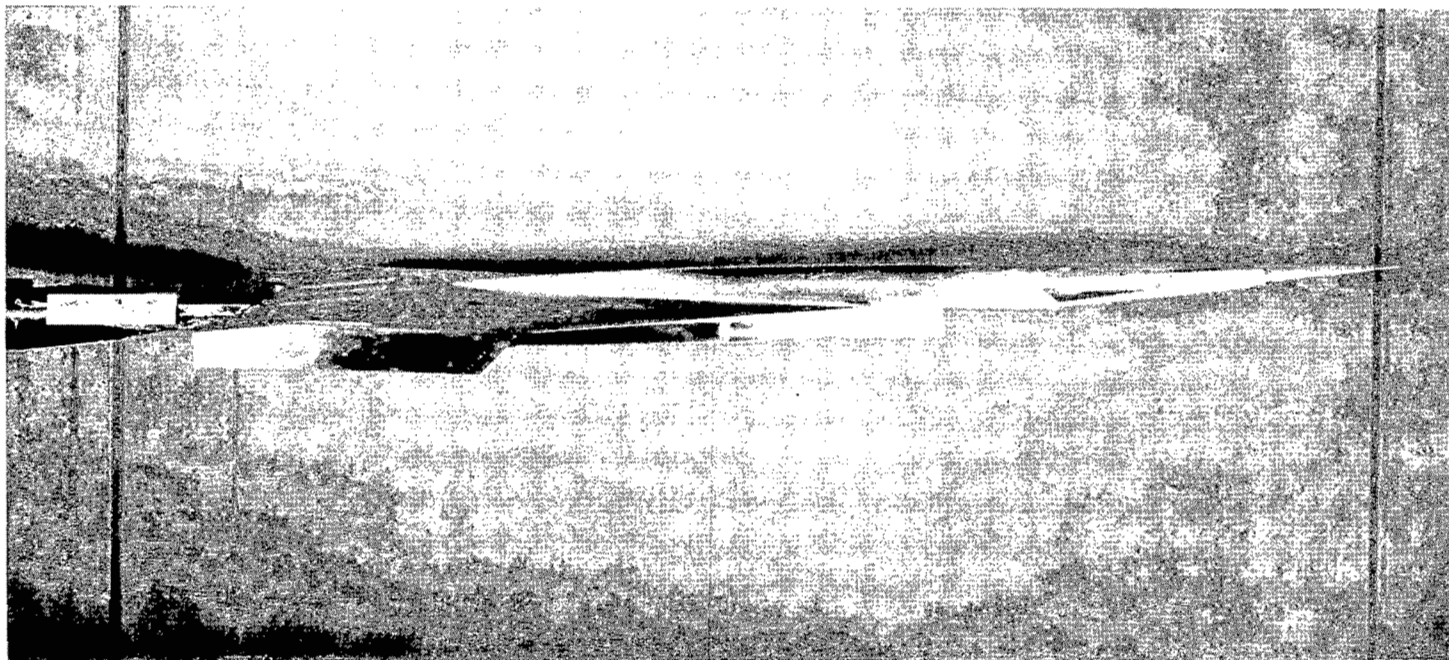
(a) Side view; original ventral fins.   L-58-250

Figure 4.- Model photographs. Modified forebody at 2.9°.
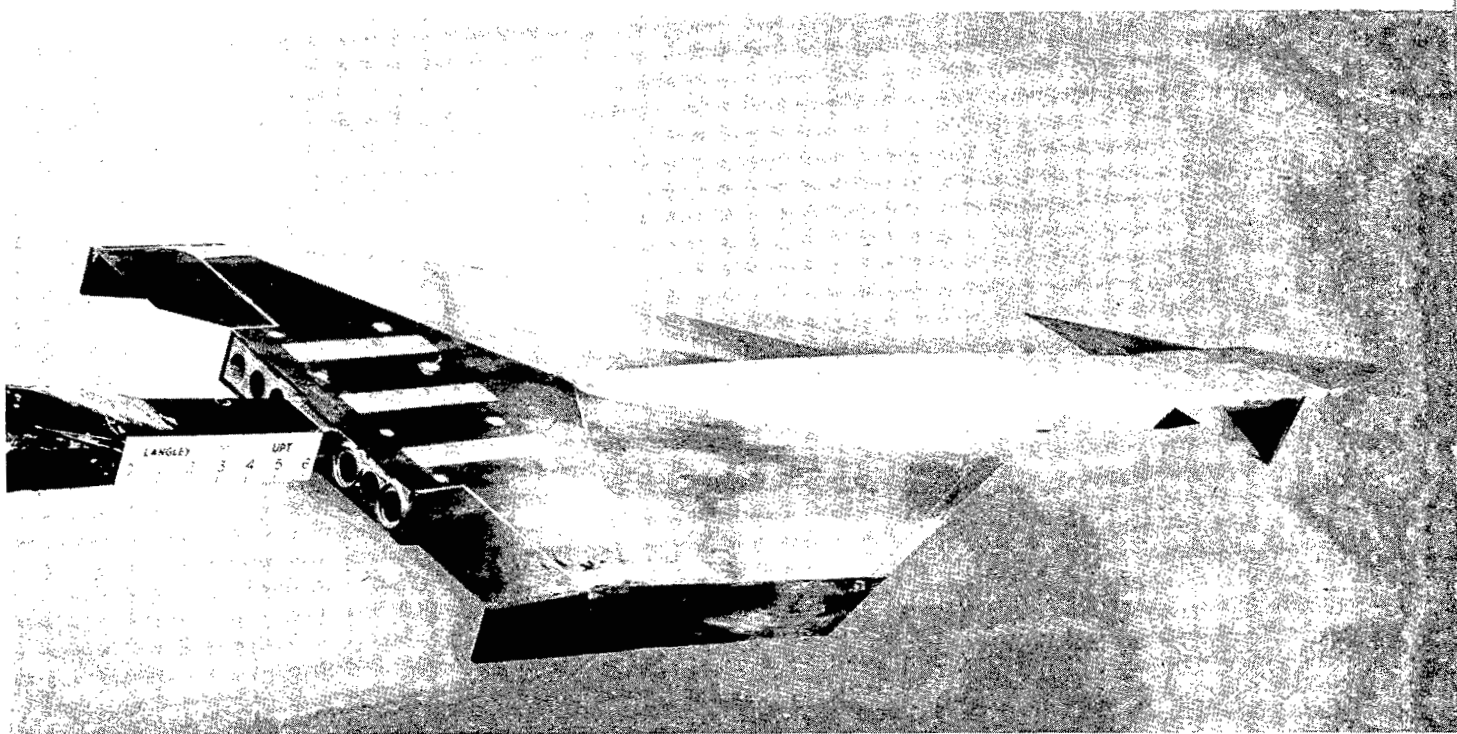
(b) Three-quarter rear view; original ventral fins.   L-58-248

Figure 4.- Continued.
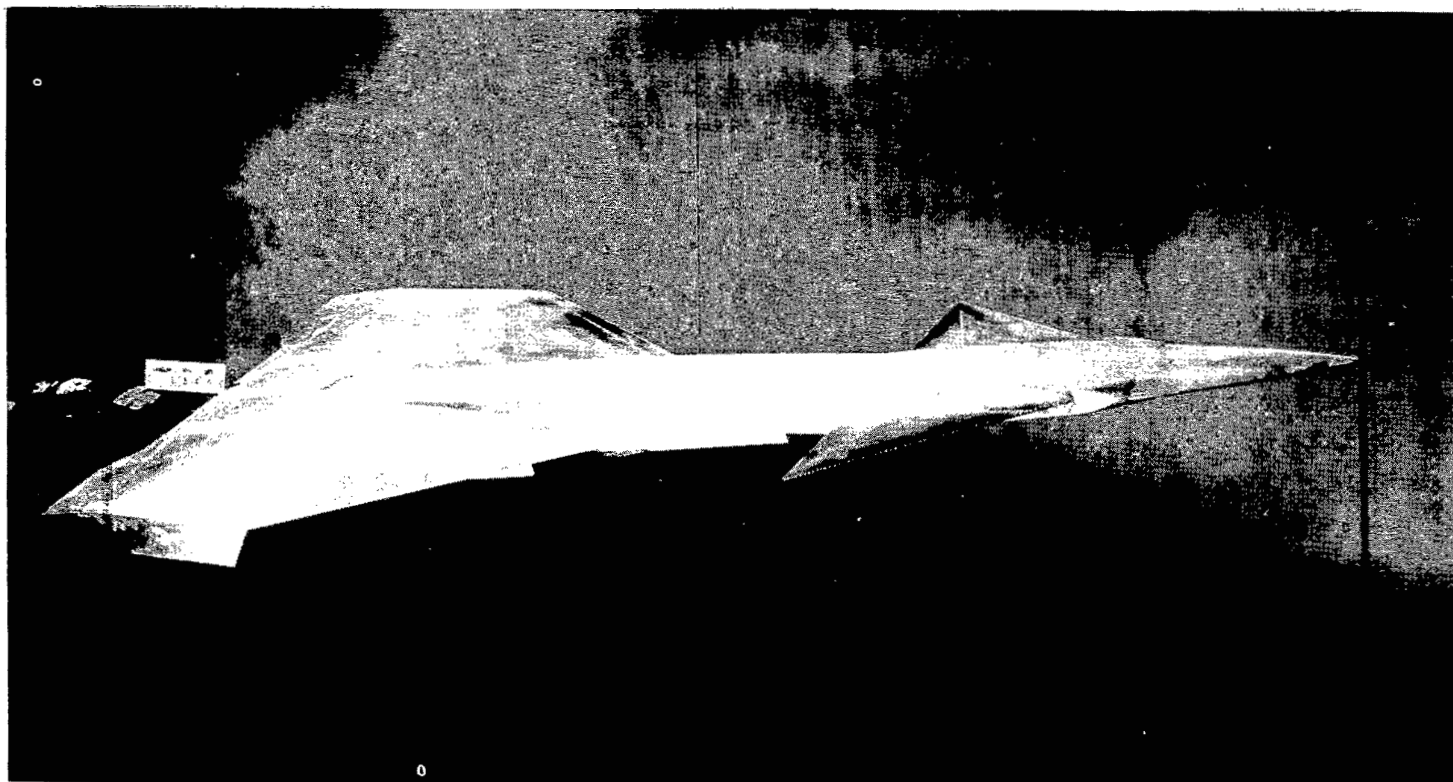
(c) Three-quarter front view; original ventral fins.   L-58-249

Figure 4.- Continued.

(d) Three-quarter front view; modified ventral fins.   L-58-252

Figure 4.- Continued.
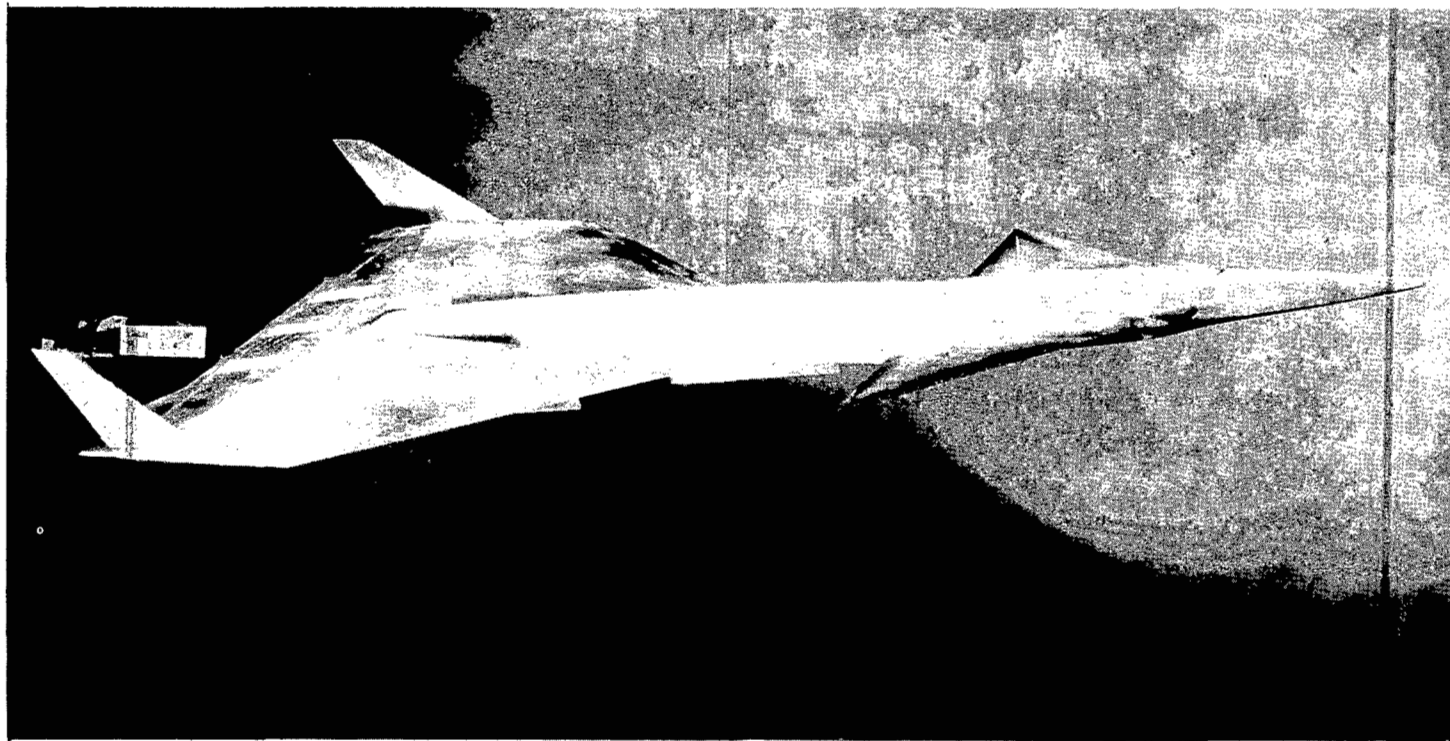
(e) Three-quarter front view; vertical fins at wing tips.   L-58-256

Figure 4.- Continued.

(f) Three-quarter front view; vertical fins at 0.3b/2.   L-58-254

Figure 4.- Concluded.

α=-4.4°

α=-.2°

α=4.0°

α=10.4°
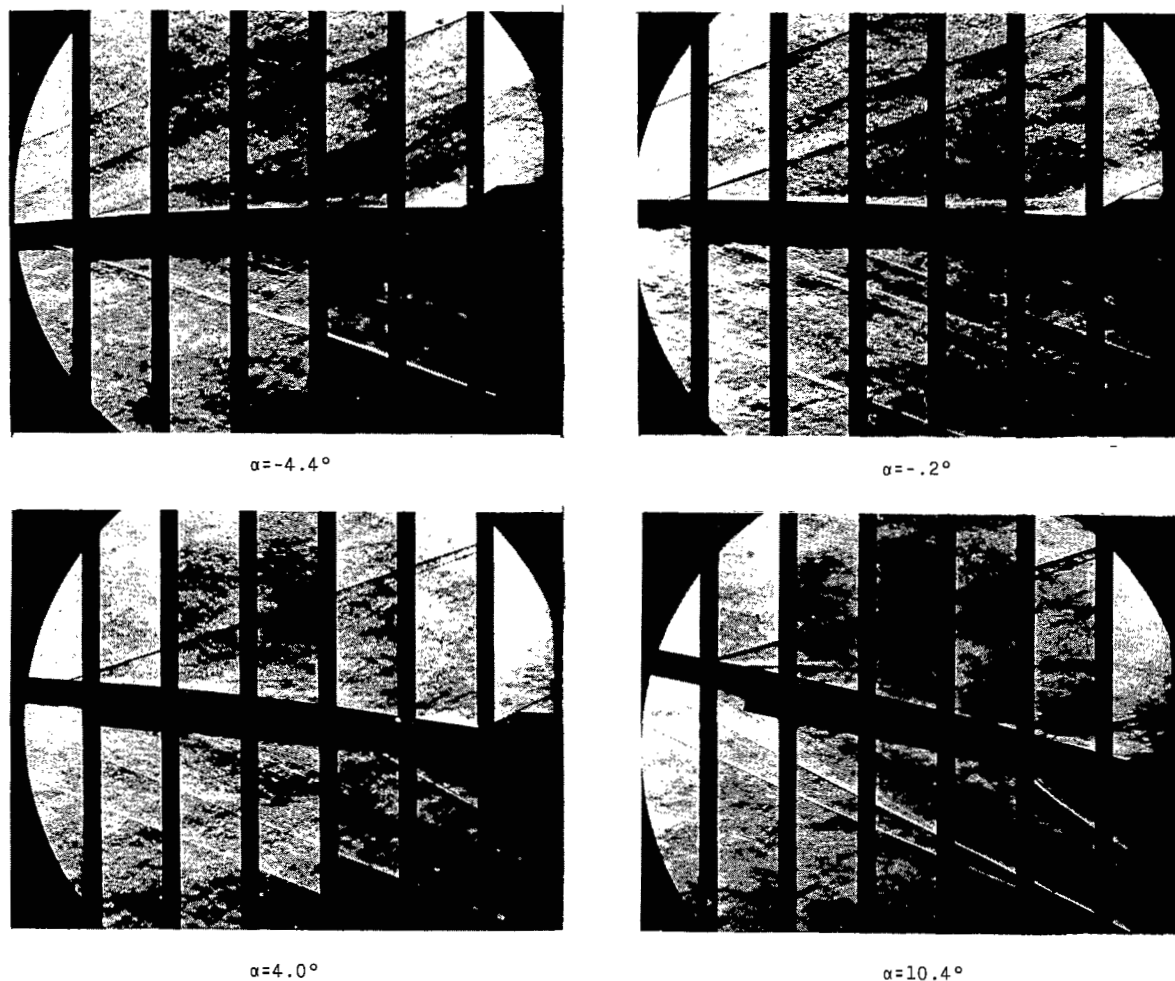
(a) Original forebody.

L-58-1699

Figure 5.- Typical schlieren photographs of model. Modified ventral fins; M = 3.00°; β = 0°.

α=-4.5°

α=-.2°

α=4.0°
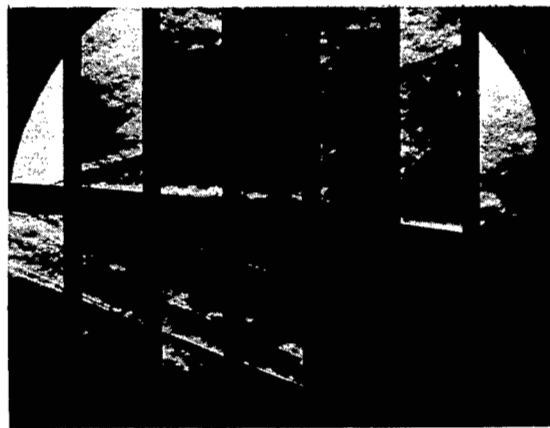
α=10.4°

(b) Modified forebody at 0°.   L-58-1700

Figure 5.- Continued.

α=-4.3°   α=-.1°
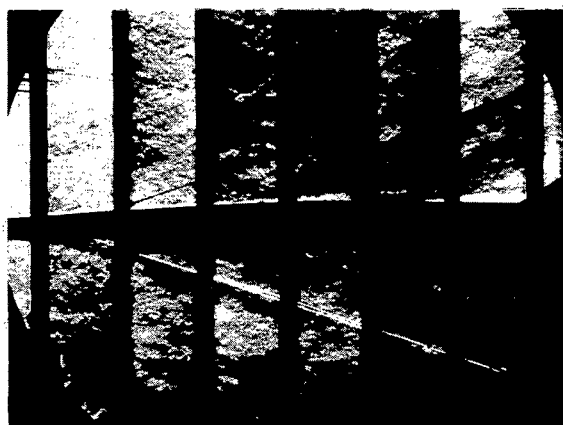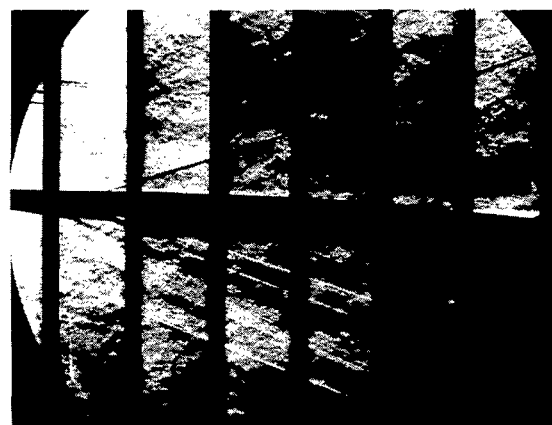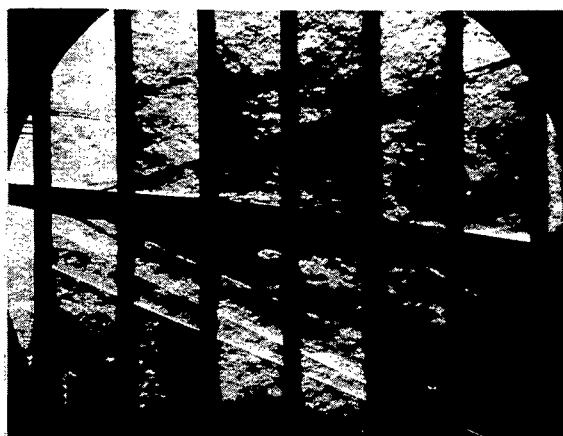
α=4.2°   α=10.6°

(c) Modified forebody at 2.9°.   L-58-2500

Figure 5.- Concluded.
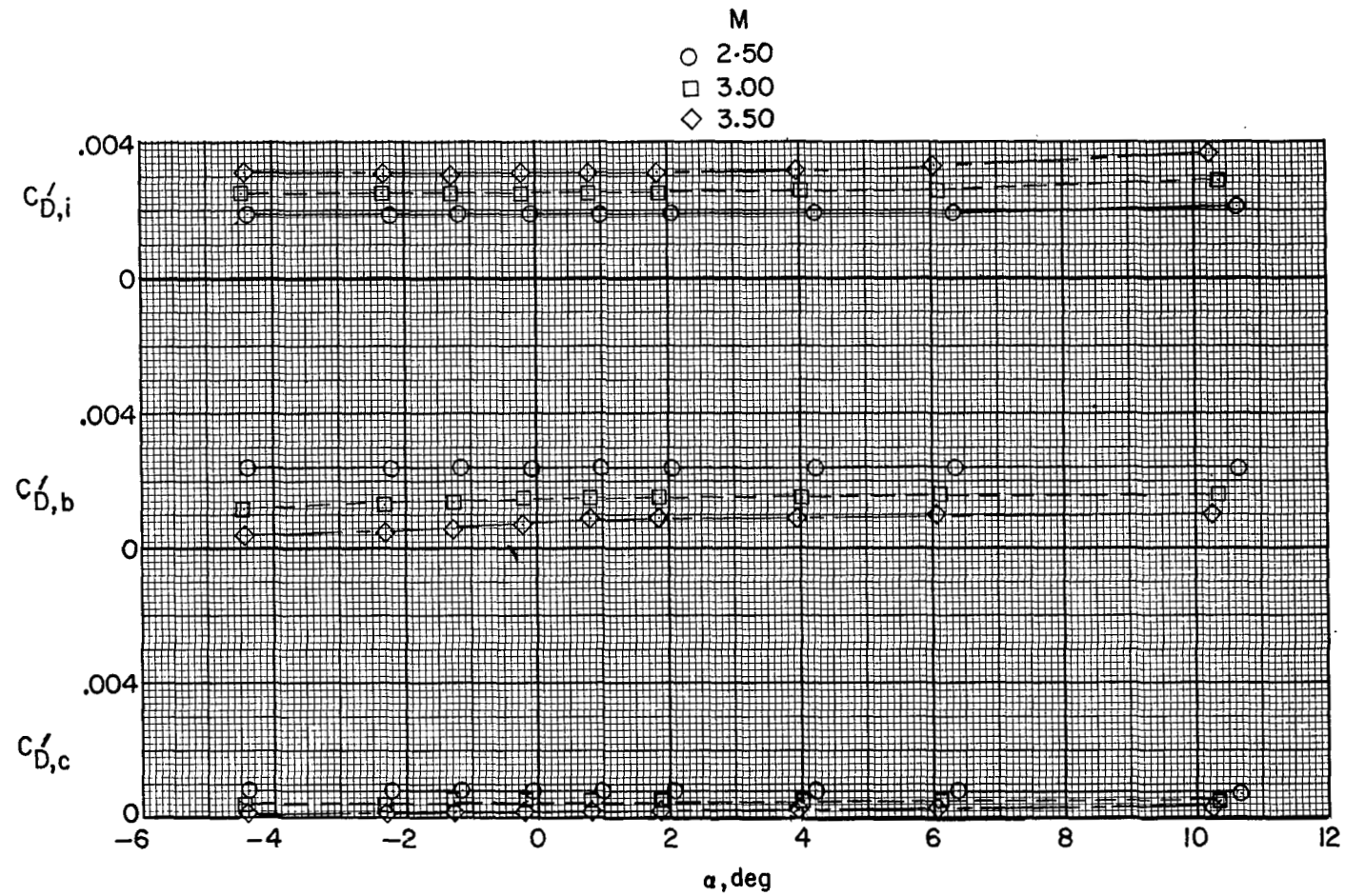
Figure 6.- Variation of internal, base, and chamber drag coefficient with angle of attack.
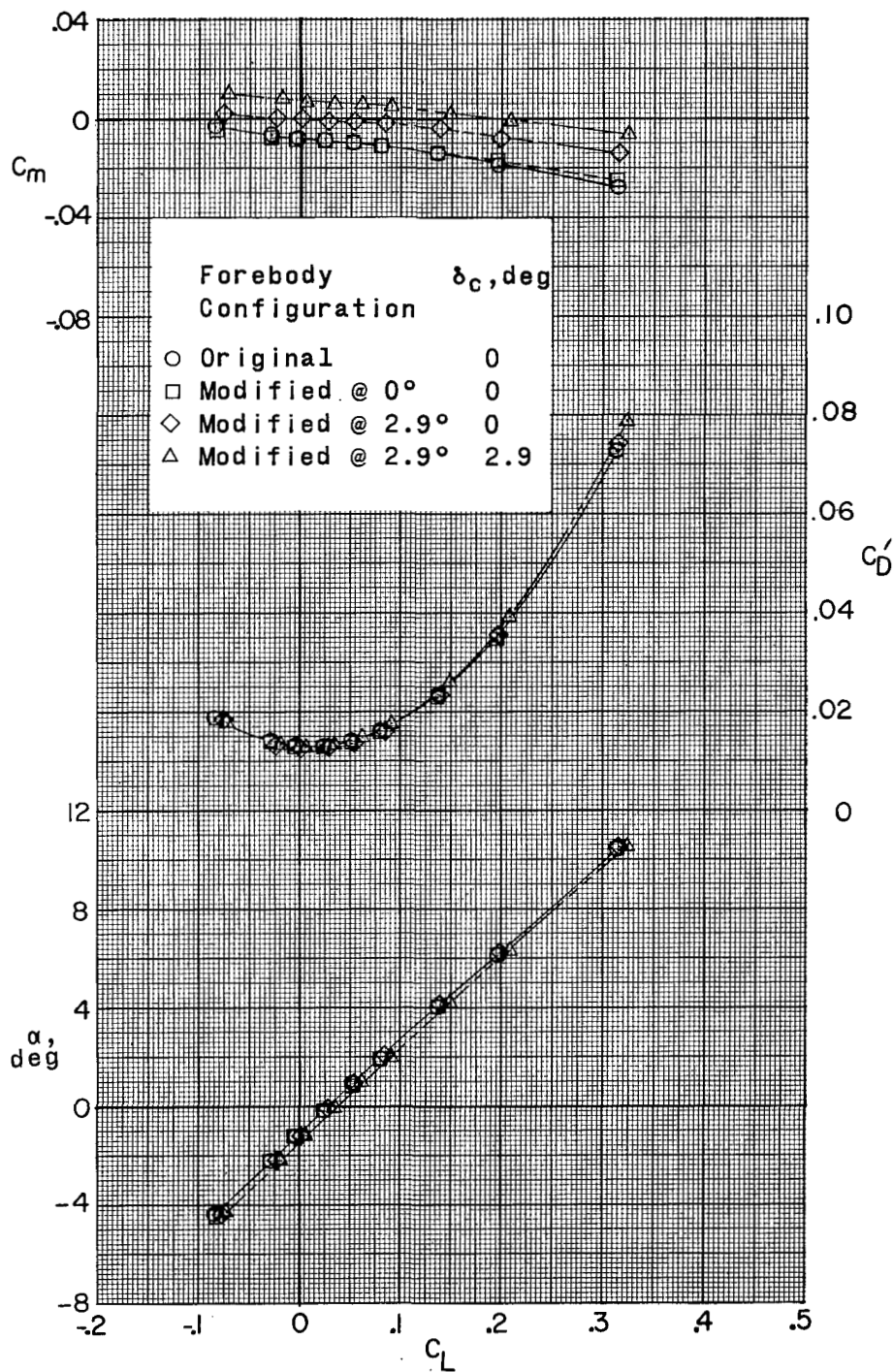
Figure 7.- Effect of forebody shape and attitude on aerodynamic charac-
teristics in pitch. Modified ventral fins; M = 3.00.
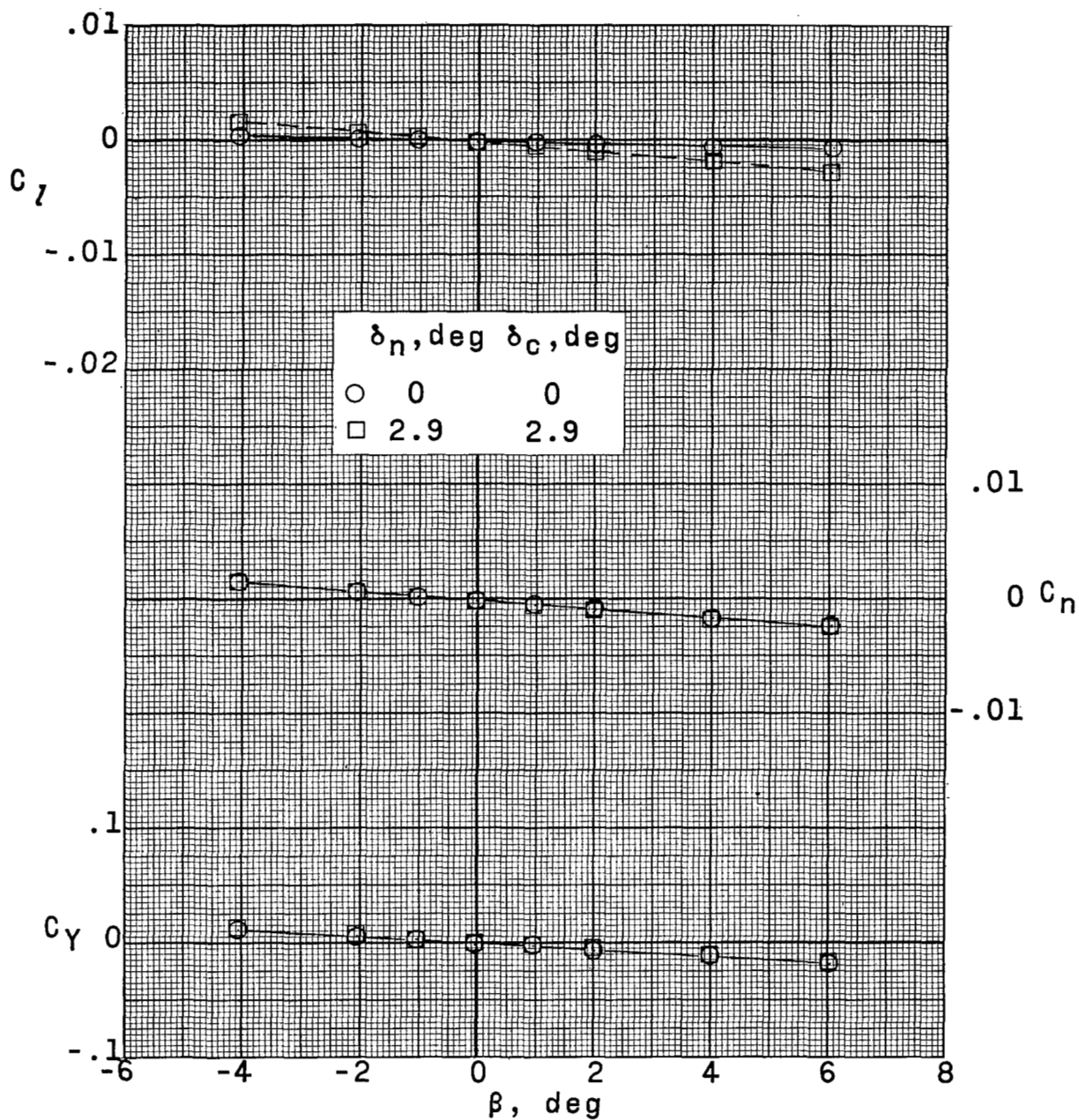
(a) $\alpha \approx 0°$.

Figure 8.- Effect of forebody and canard attitude on aerodynamic charac-
teristics in sideslip. Modified forebody; original ventral fins;
M = 3.00.
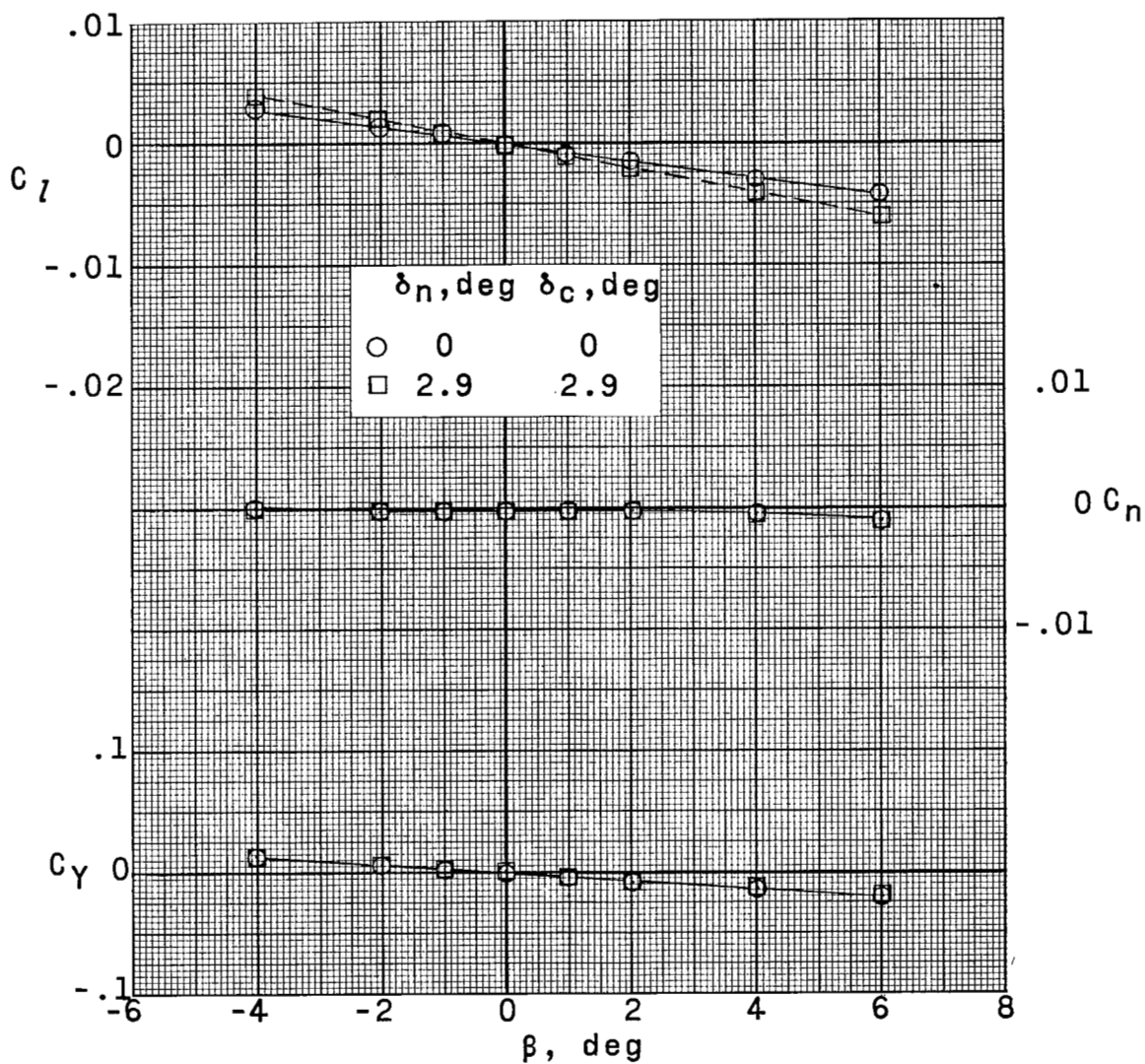
(b) $\alpha \approx 4°$.

Figure 8.- Continued.
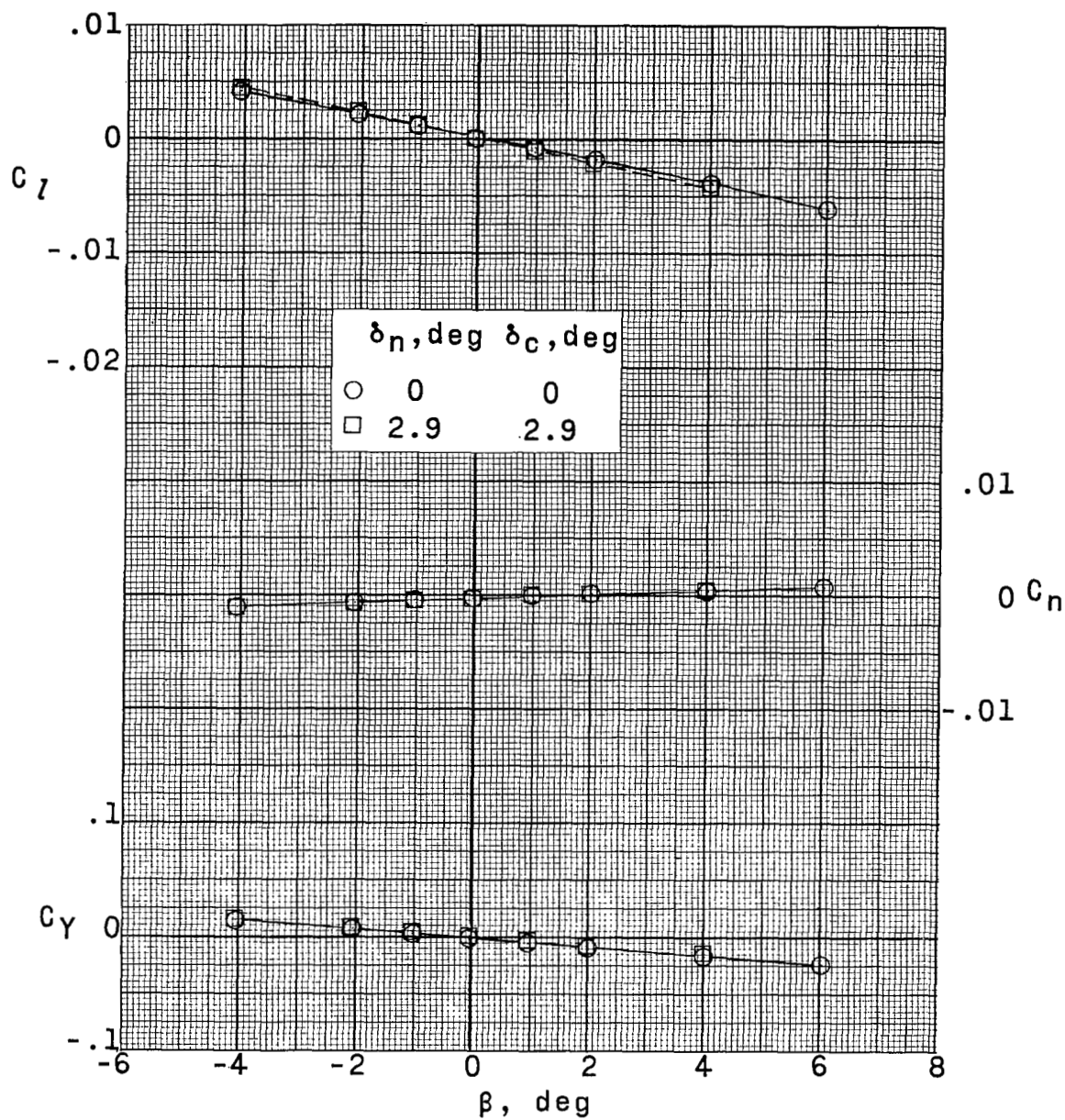
(c) $\alpha \approx 10^\circ$.

Figure 8.- Concluded.
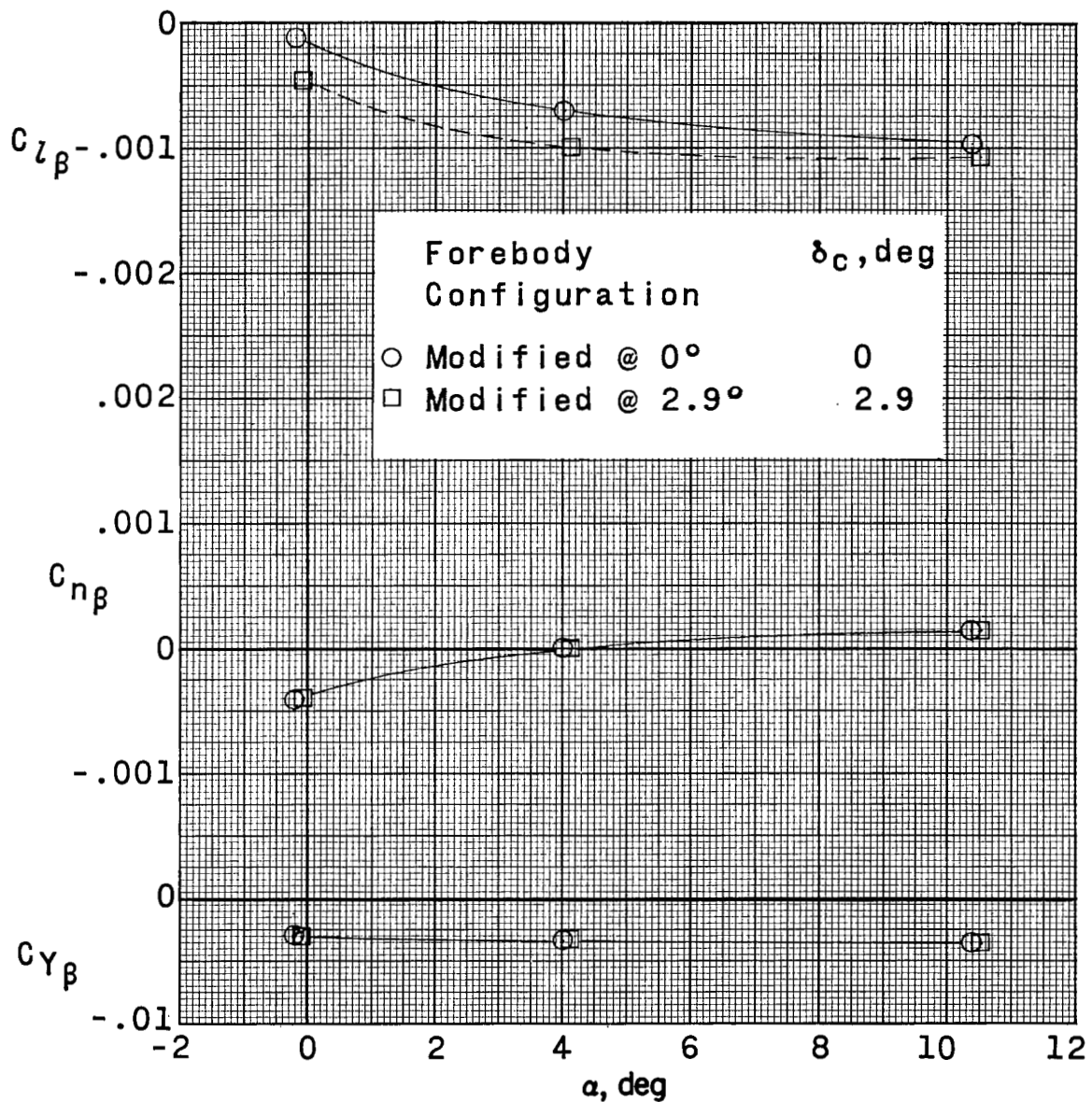
Figure 9.- Effect of forebody and canard deflection on the static lateral
   and directional stability derivatives with angle of attack. Original
   ventral fins; M = 3.00.
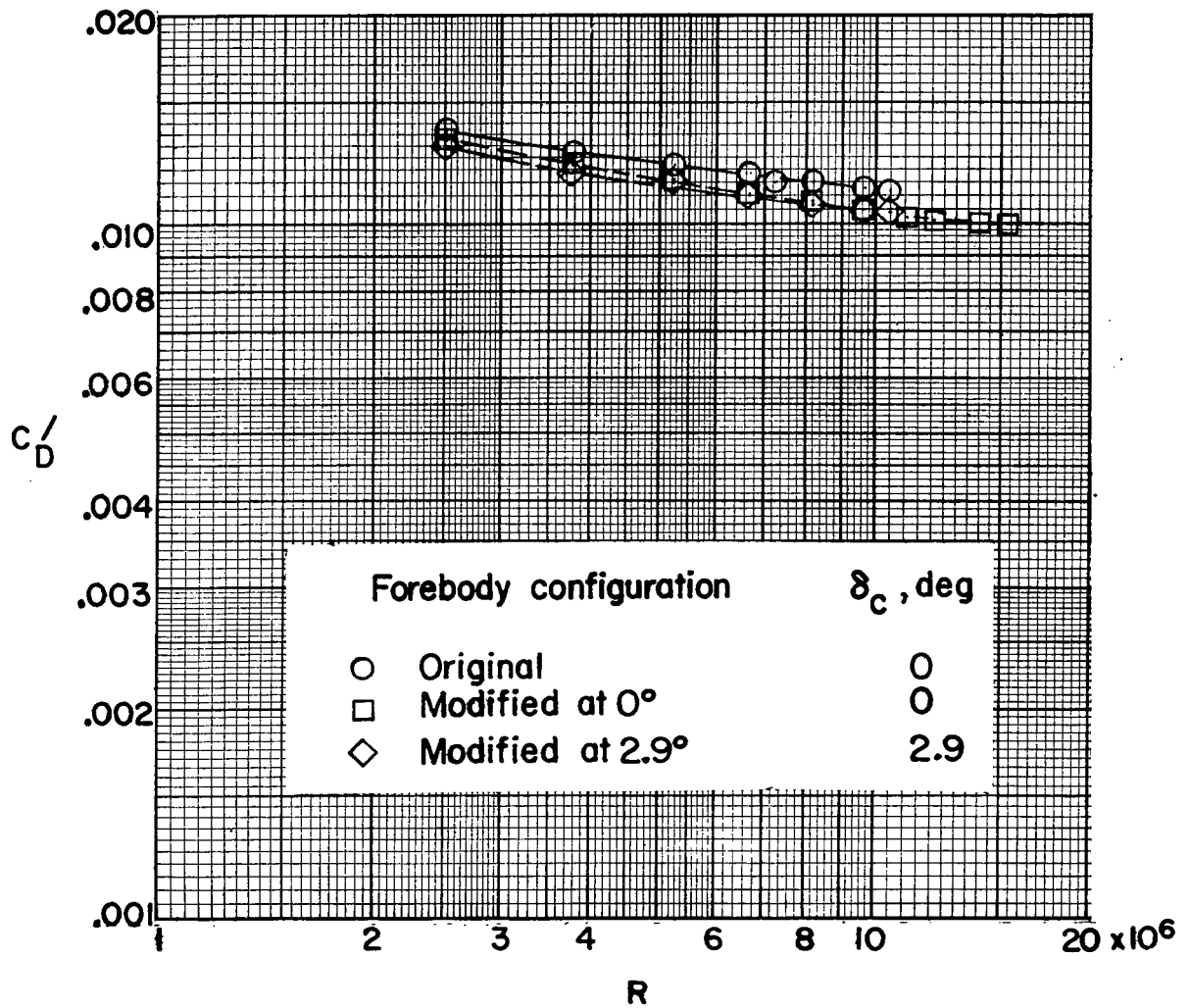
Figure 10.- Effect of variation of Reynolds number on minimum drag coefficient for the three test forebodies. Modified ventral fins; transition fixed (0.031" grain size); M = 3.00.
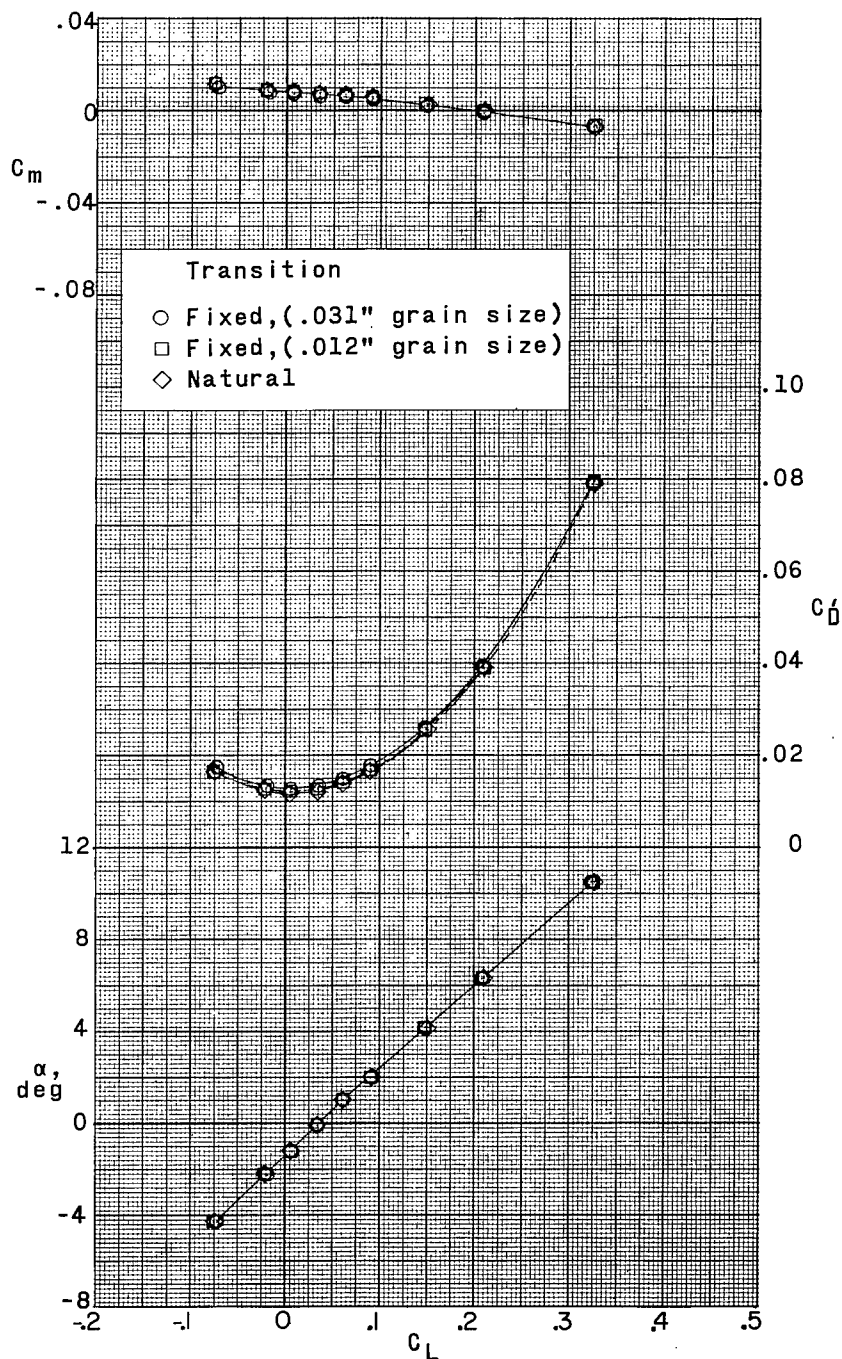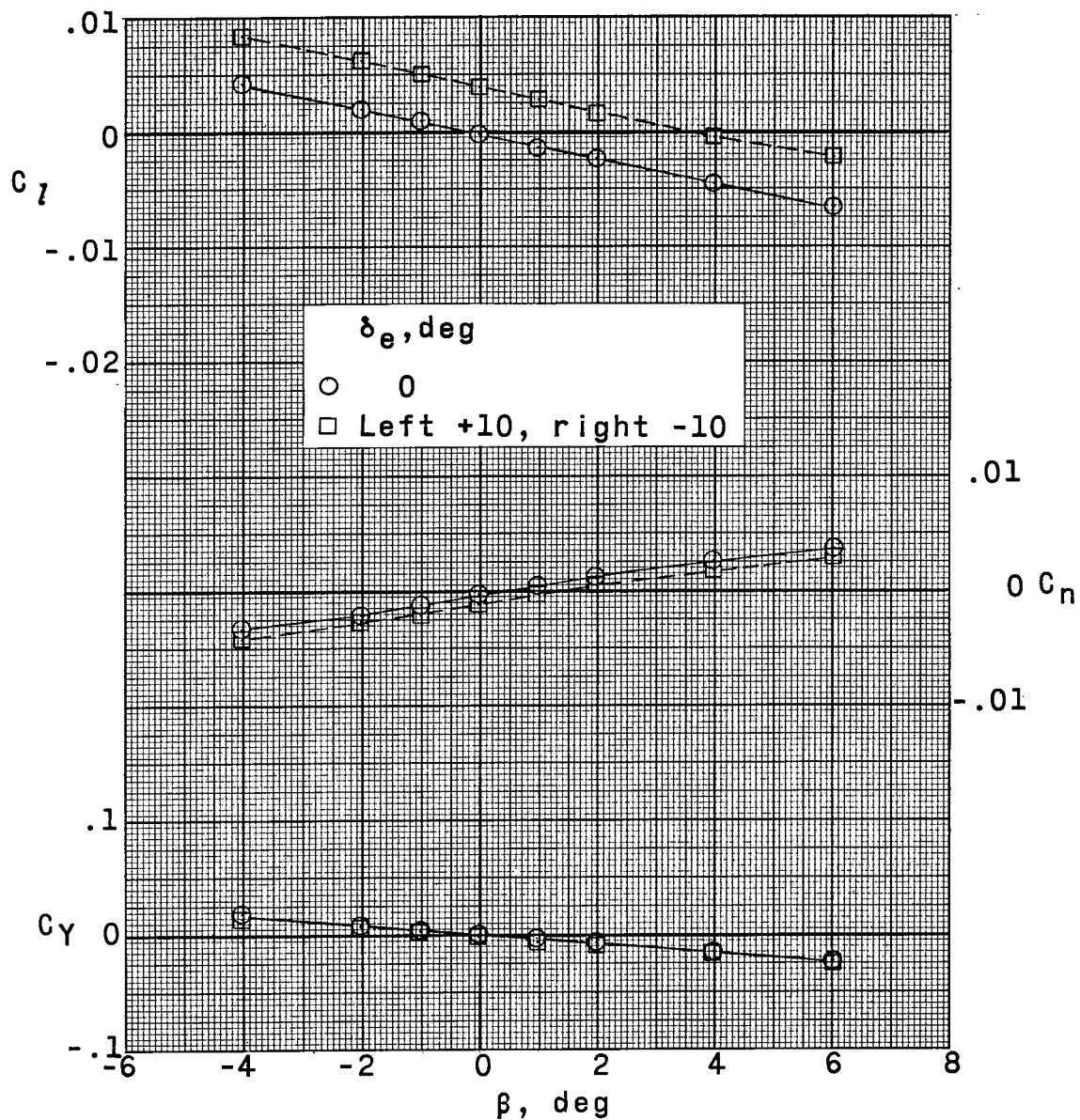
Figure 11.- Effect of transition on aerodynamic characteristics in pitch. Modified forebody at 2.9°; δ_c = 2.9°; modified ventral fins; M = 3.00.

Figure 12.- Effect of variation of Reynolds number on minimum drag coefficient for various transition conditions. Modified forebody at $2.9°$; $\delta_c = 2.9°$; modified ventral fins; $M = 3.00$.
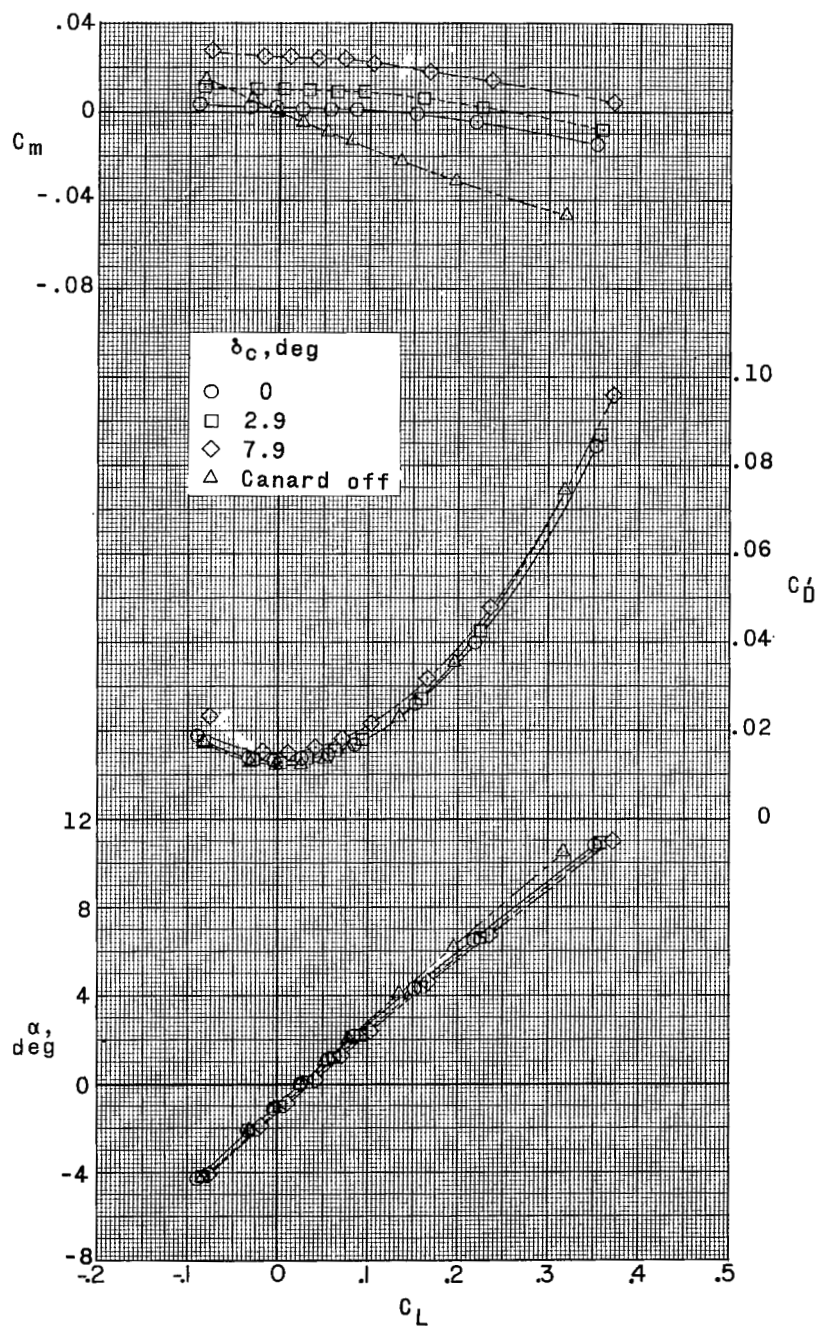
(a) M = 2.50.

Figure 13.- Effect of canard on aerodynamic characteristics in pitch.
Modified forebody at 2.9°; original ventral fins.
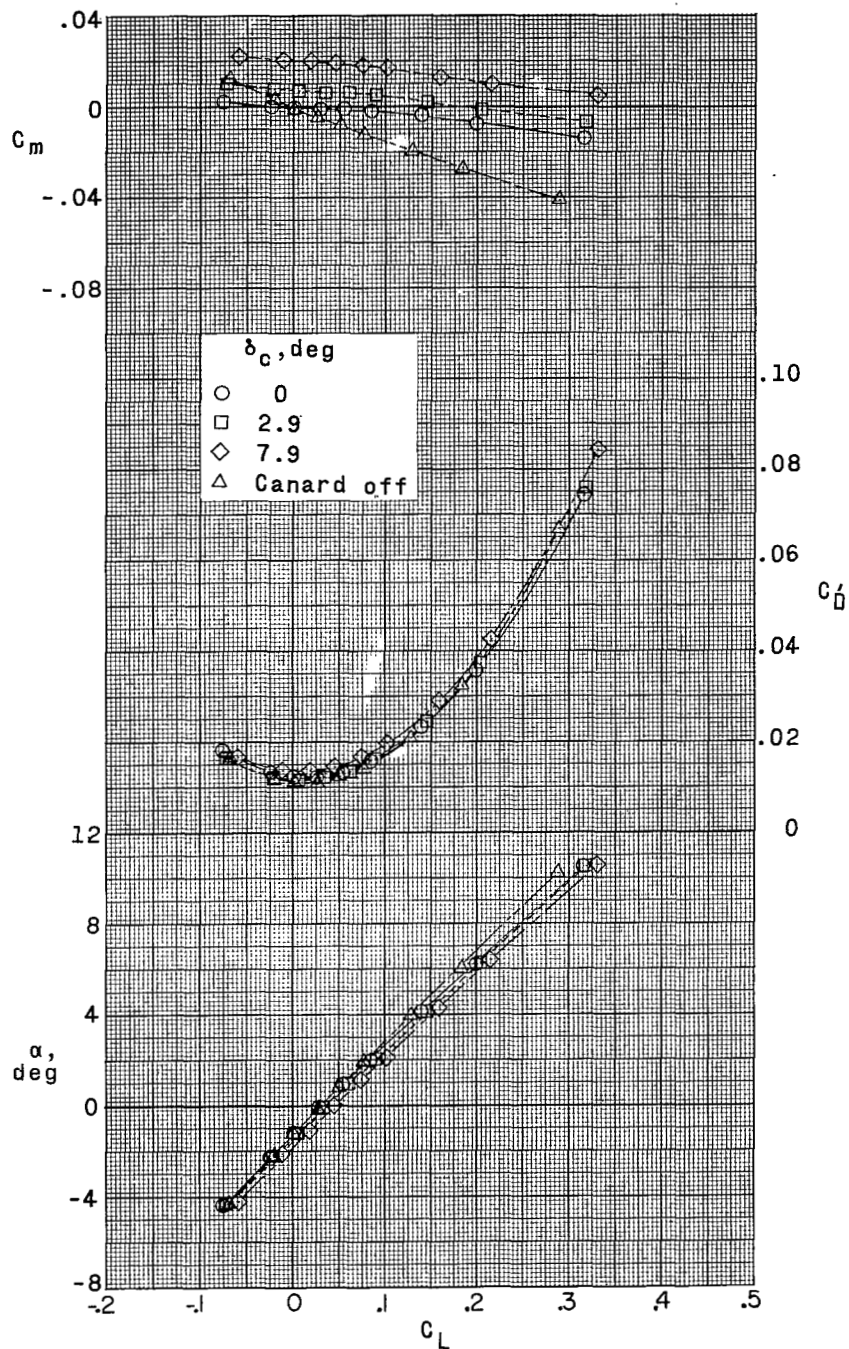
(b) M = 3.00.

Figure 13.- Continued.
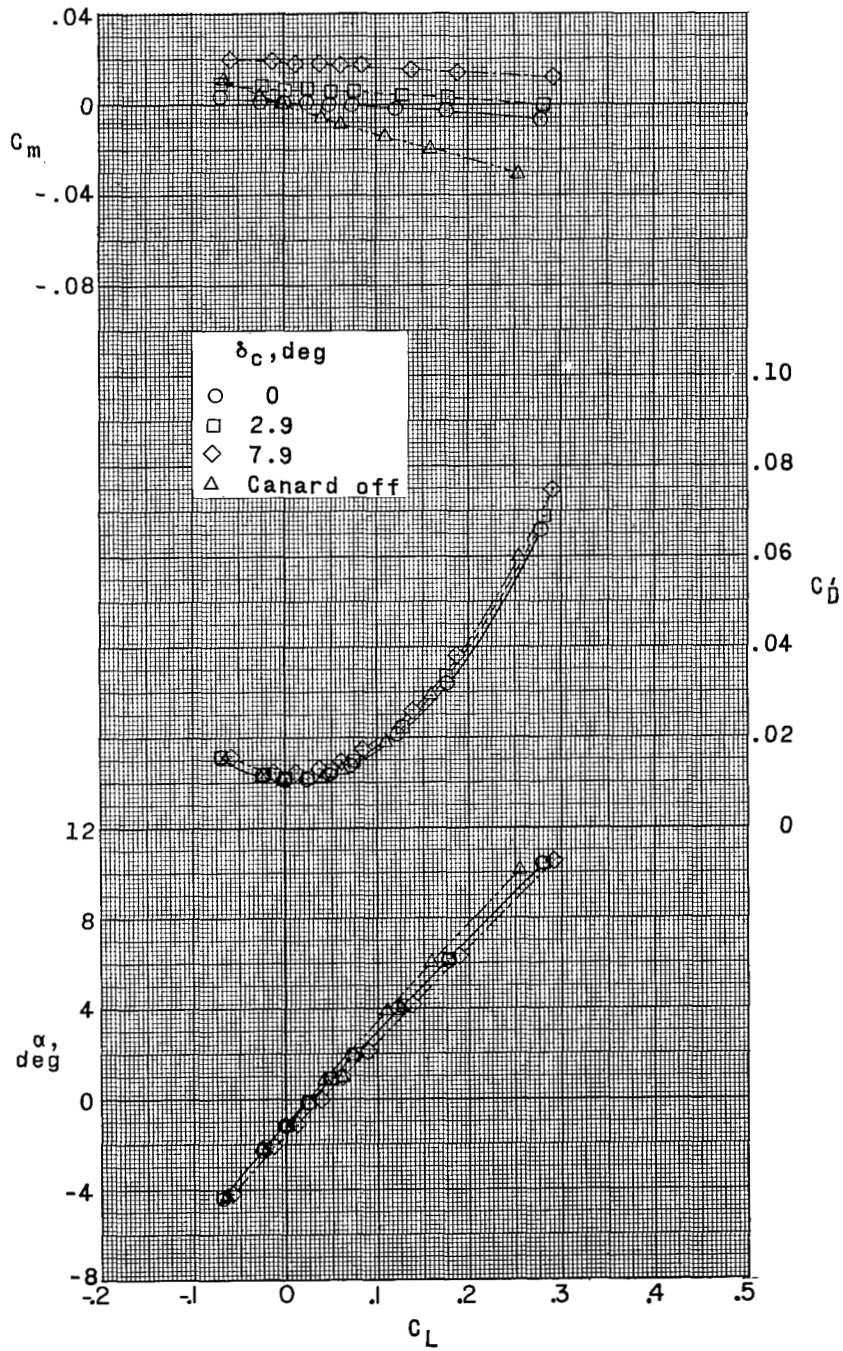
(c)   M = 3.50.

Figure 13.- Concluded.
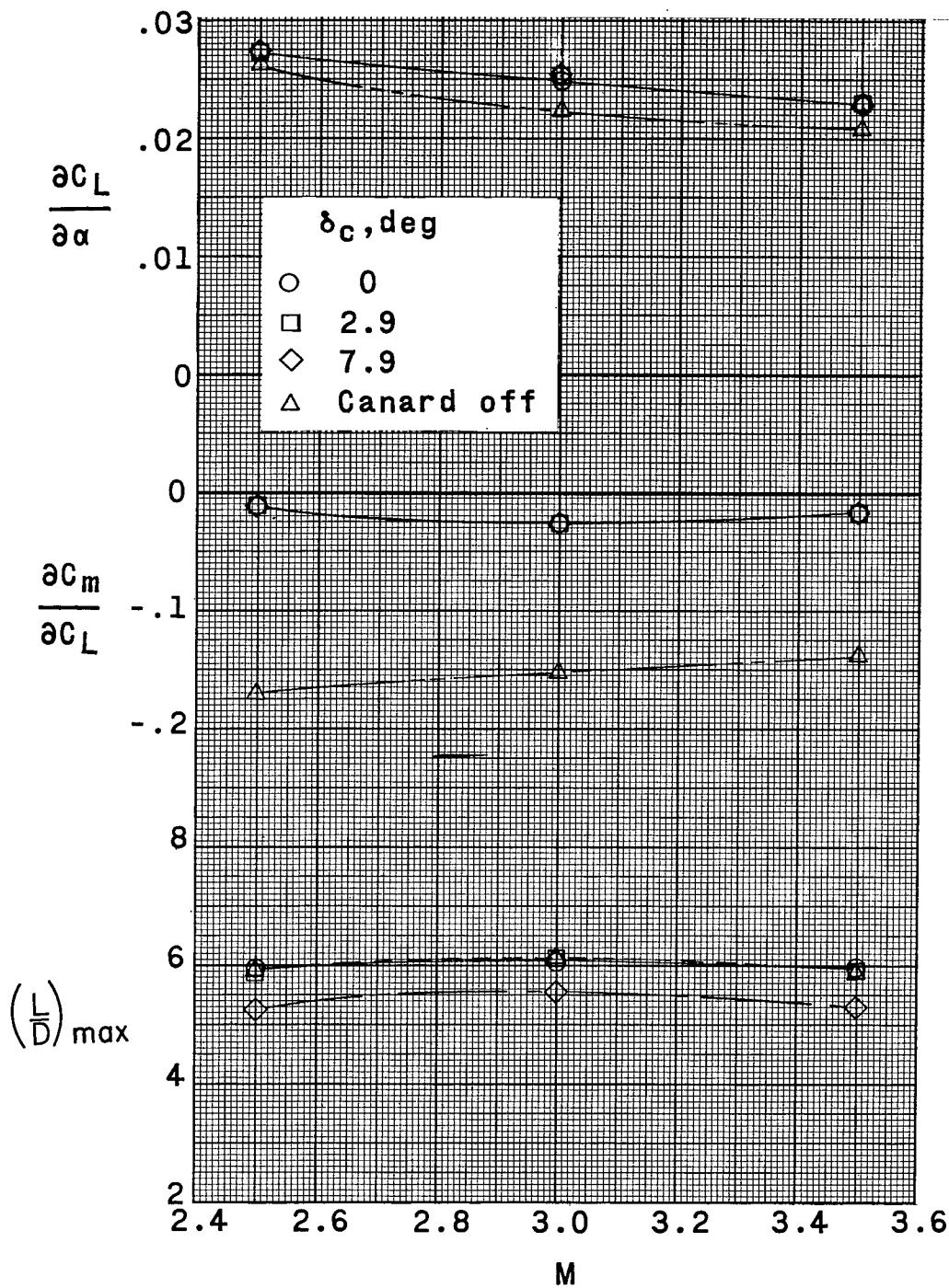
Figure 14.- Summary of aerodynamic characteristics in pitch. Effect of
canard. Original ventral fins; forebody at 2.9°.
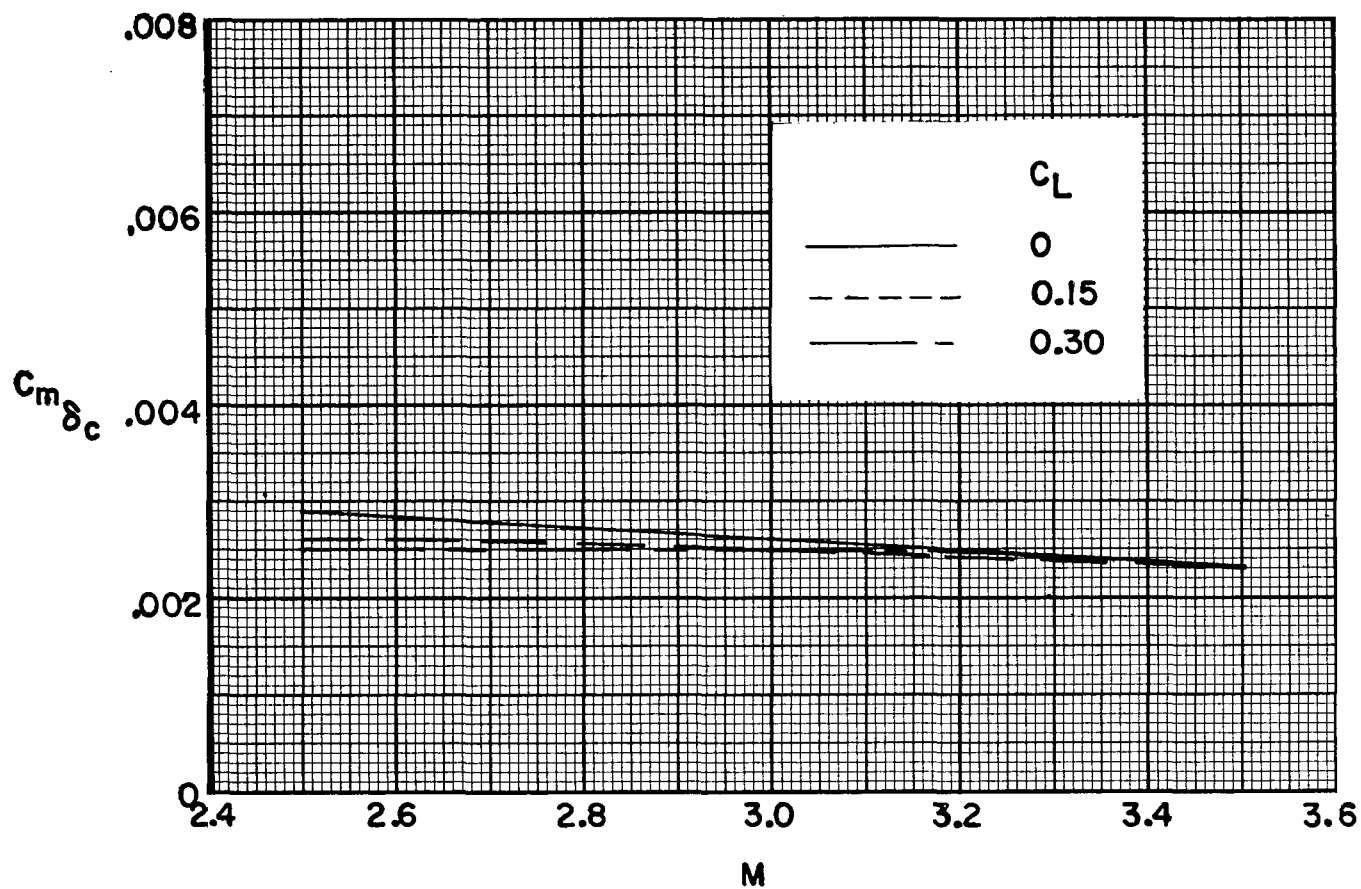
Figure 15.- Variation of canard effectiveness with Mach number for several lift coefficients. Modified forebody at 2.9°; original ventral fins.
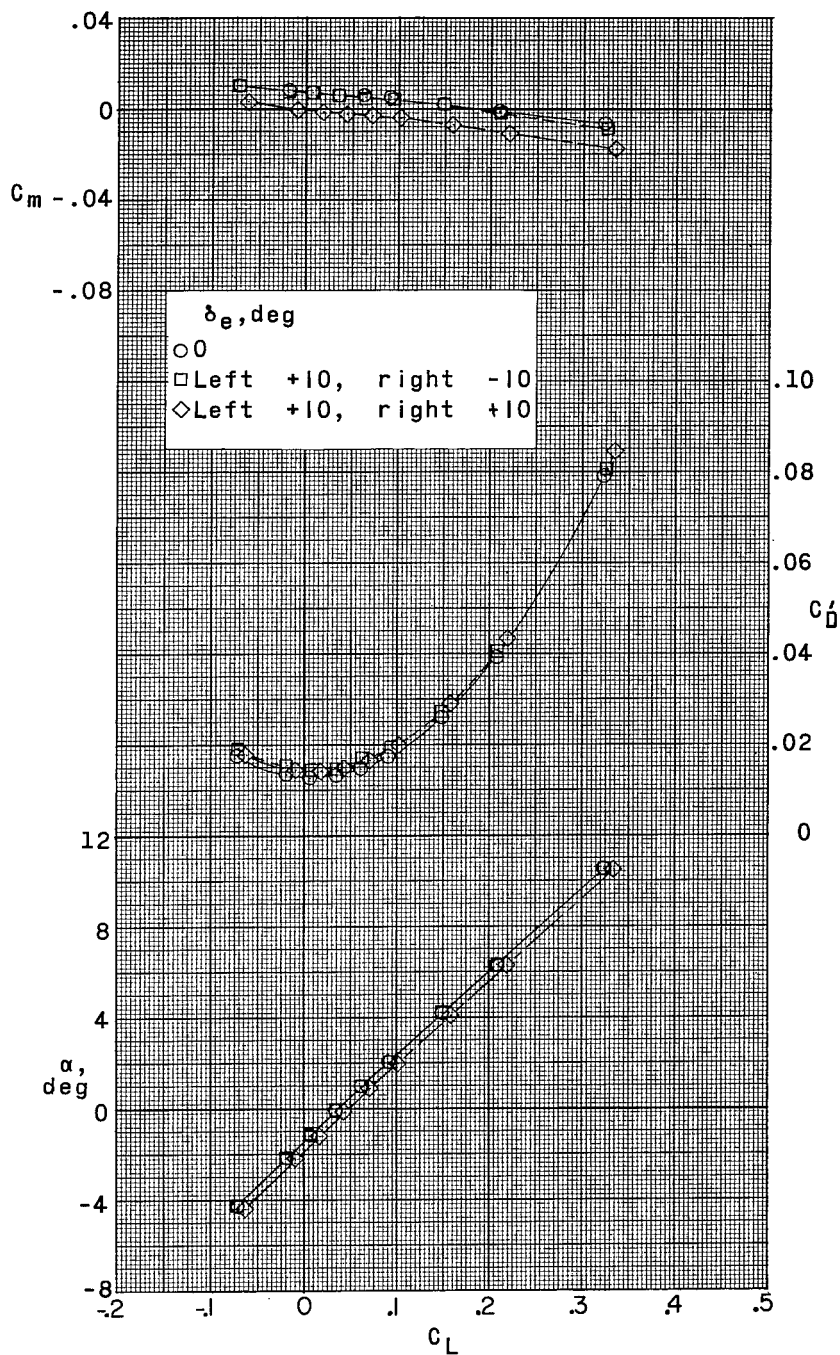
Figure 16.- Effect of elevon deflection on aerodynamic characteristics
in pitch. Modified forebody at 2.9°; δ_c = 2.9°; modified ventral
fins; M = 3.00.

(a) $\alpha \approx 0^{O}$.

Figure 17.- Effect of elevon deflection on aerodynamic characteristics in sideslip. Modified forebody at 2.9^{O}; $\delta_c = 2.9^{O}$; modified ventral fins; M = 3.00.

(b) $\alpha \approx 4^{\circ}$.

Figure 17.- Continued.
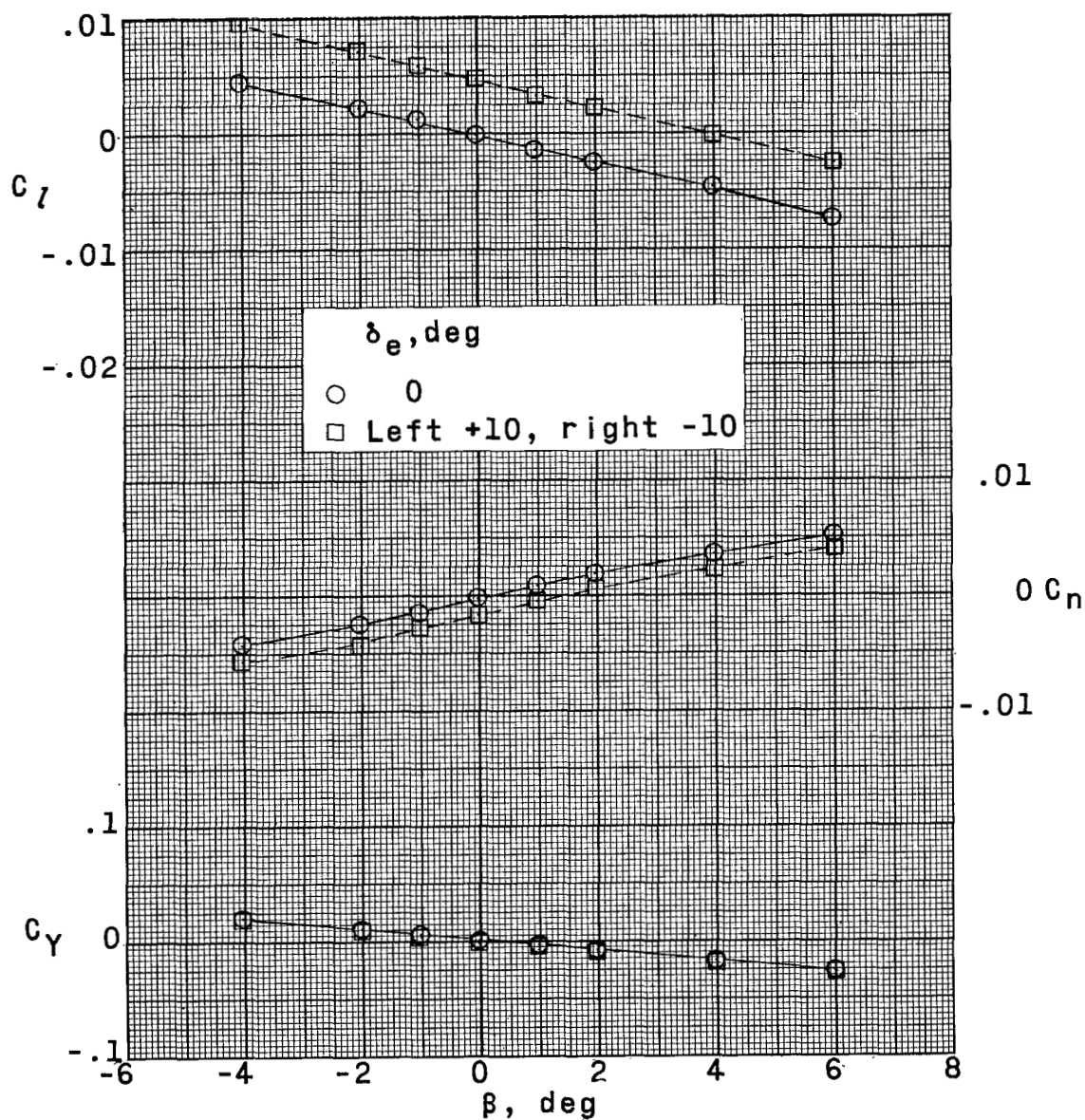
(c) $\alpha \approx 10^{\circ}$.

Figure 17.- Concluded.
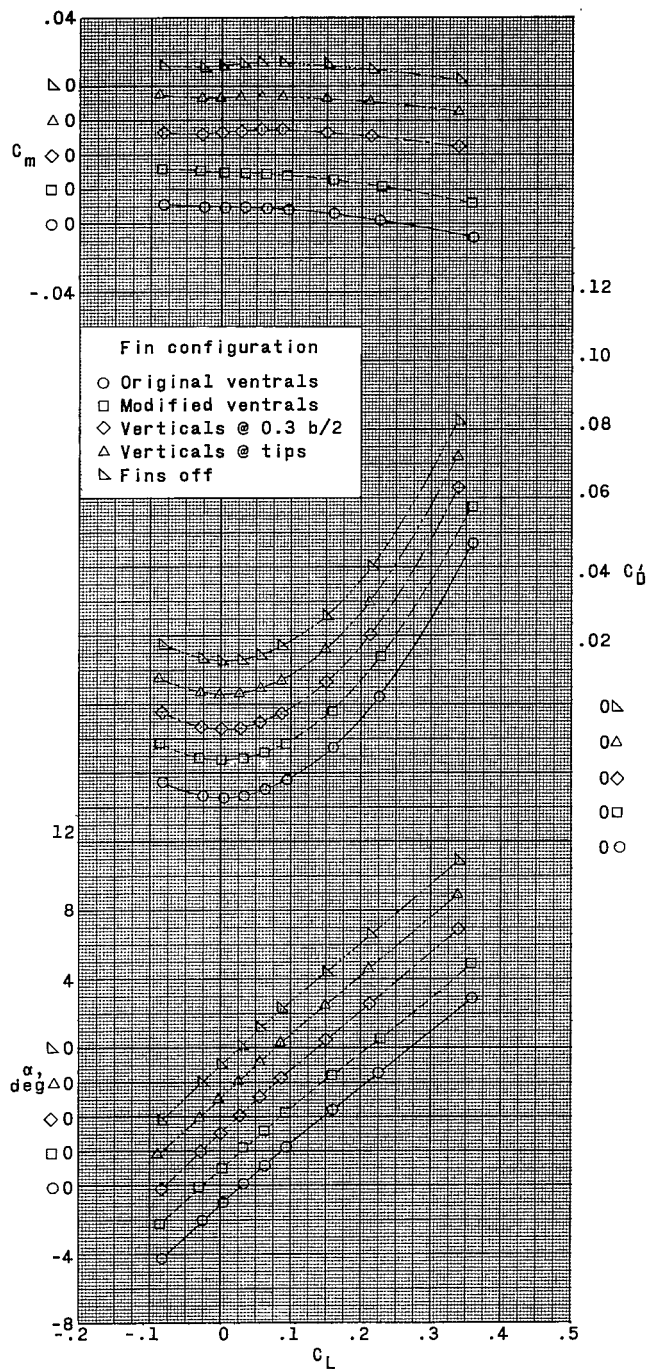
(a) M = 2.50.

Figure 18.- Effect of ventral and vertical fins on aerodynamic character-
istics in pitch. Modified forebody at 2.9°; δ_c = 2.9°.
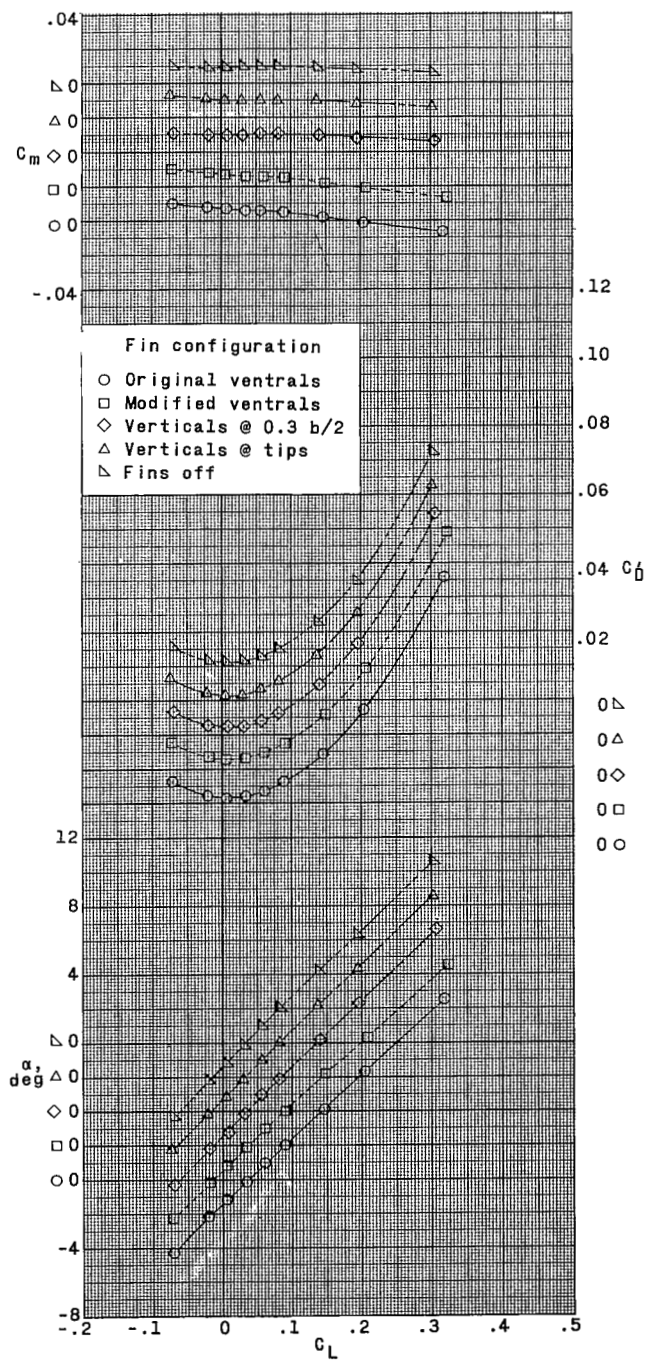
(b) M = 3.00.

Figure 18.- Continued.

Fin configuration
○ Original ventrals
□ Modified ventrals
◇ Verticals @ 0.3 b/2
△ Verticals @ tips
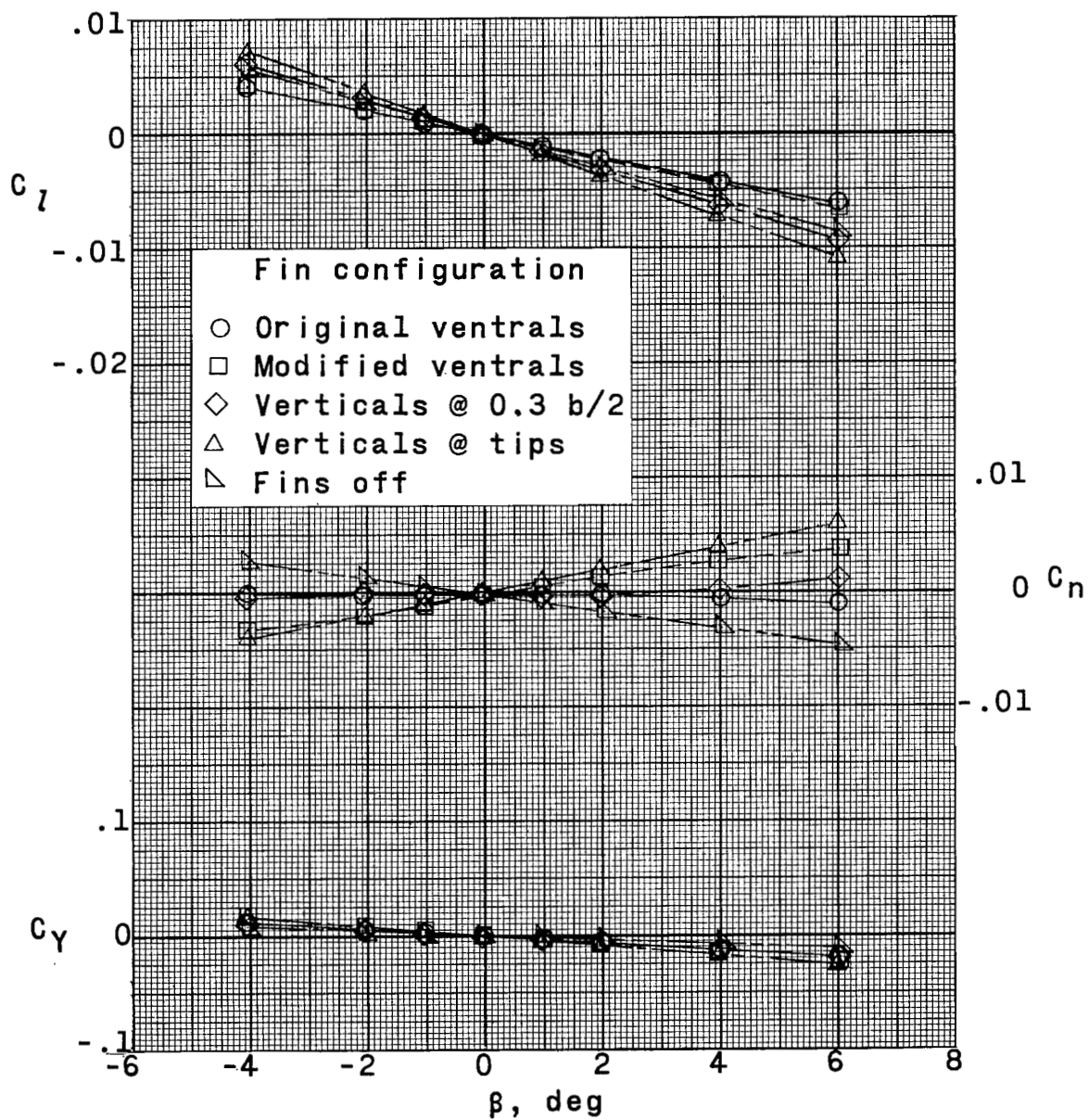◁ Fins off
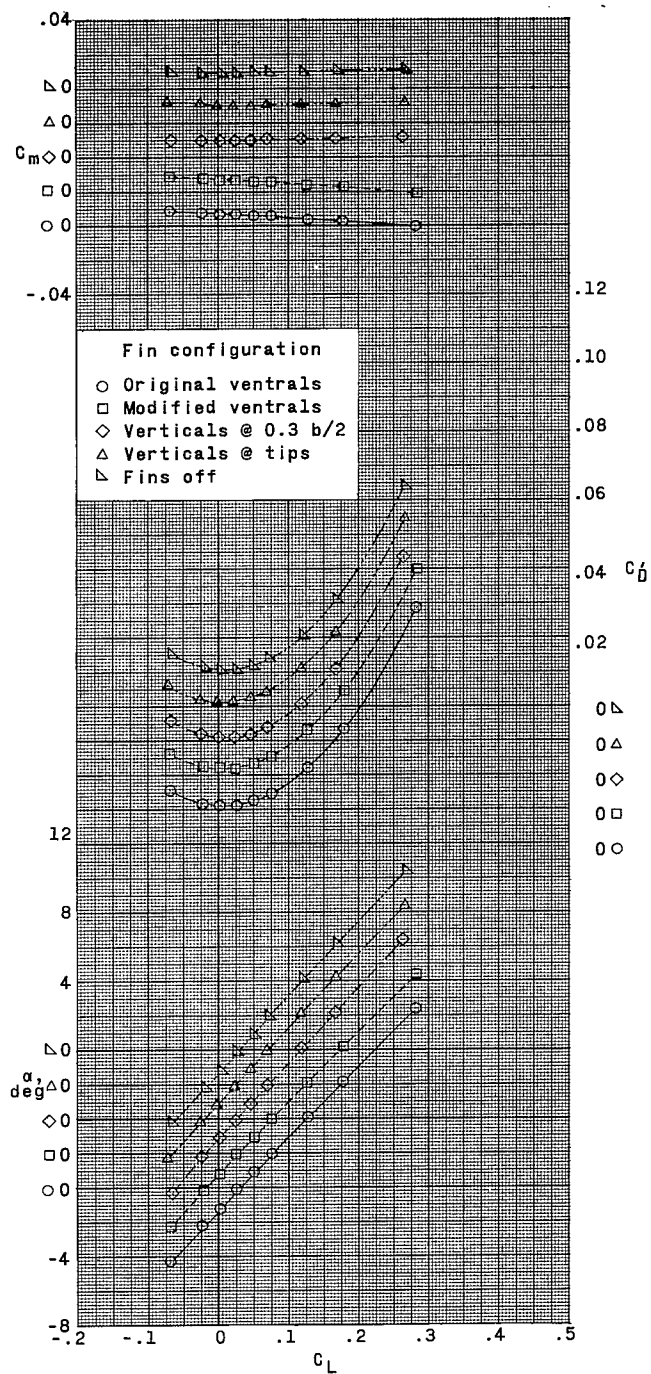
(c)   M = 3.50.

Figure 18.- Concluded.
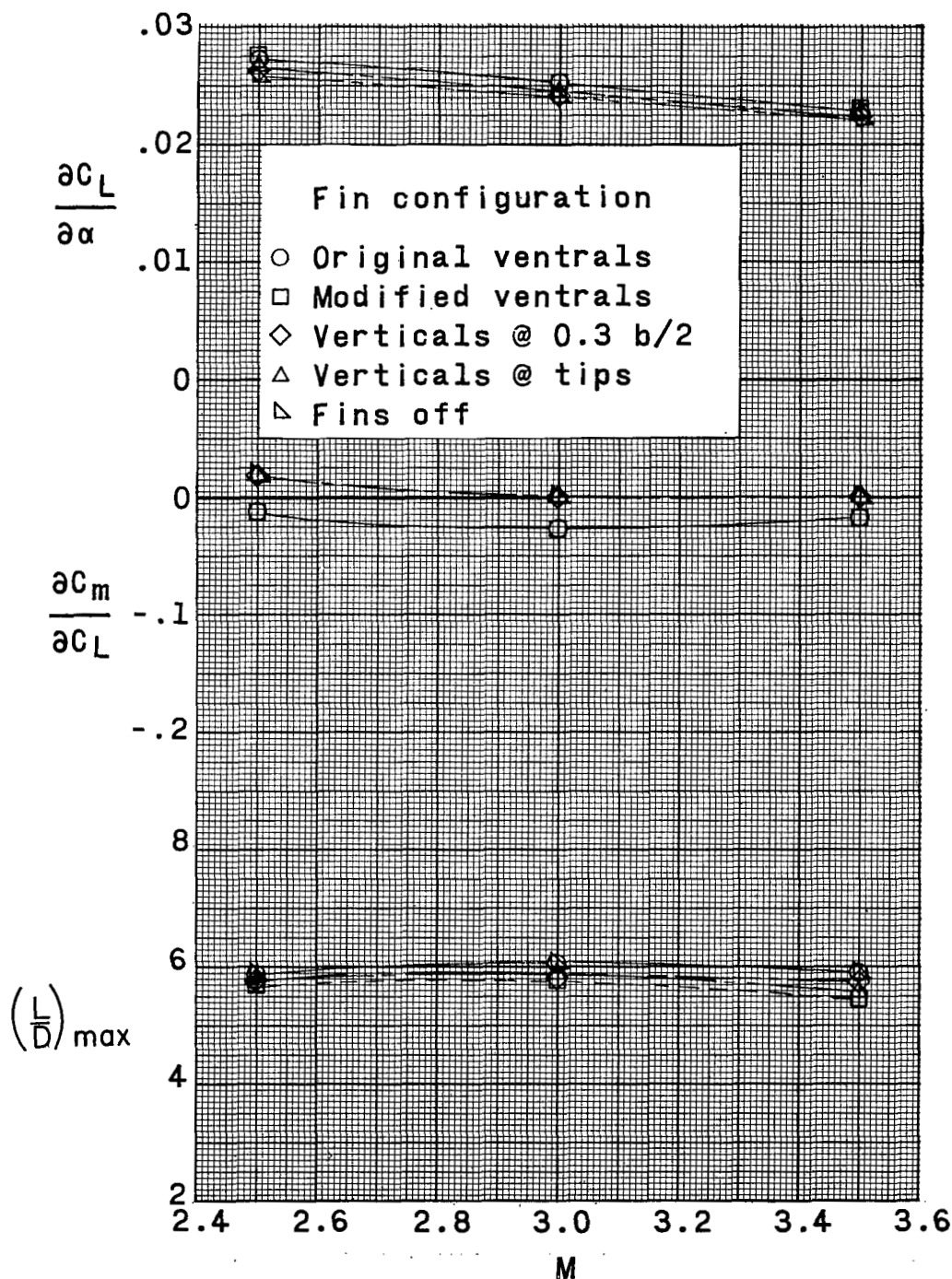
Figure 19.- Summary of aerodynamic characteristics in pitch. Effect of ventral and vertical fins. Modified forebody at 2.9°.
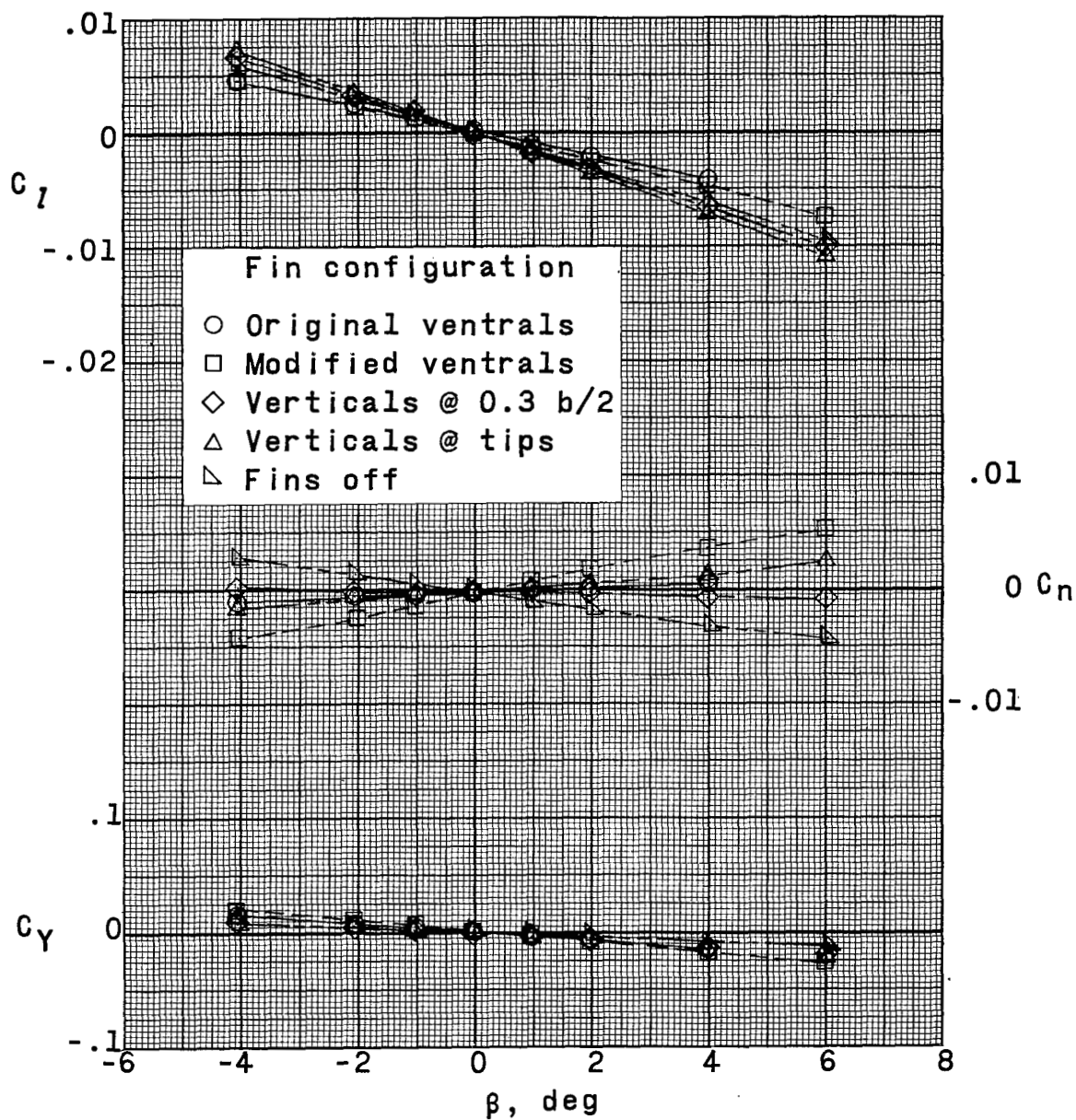
(a) $\alpha \approx 0^{o}$.
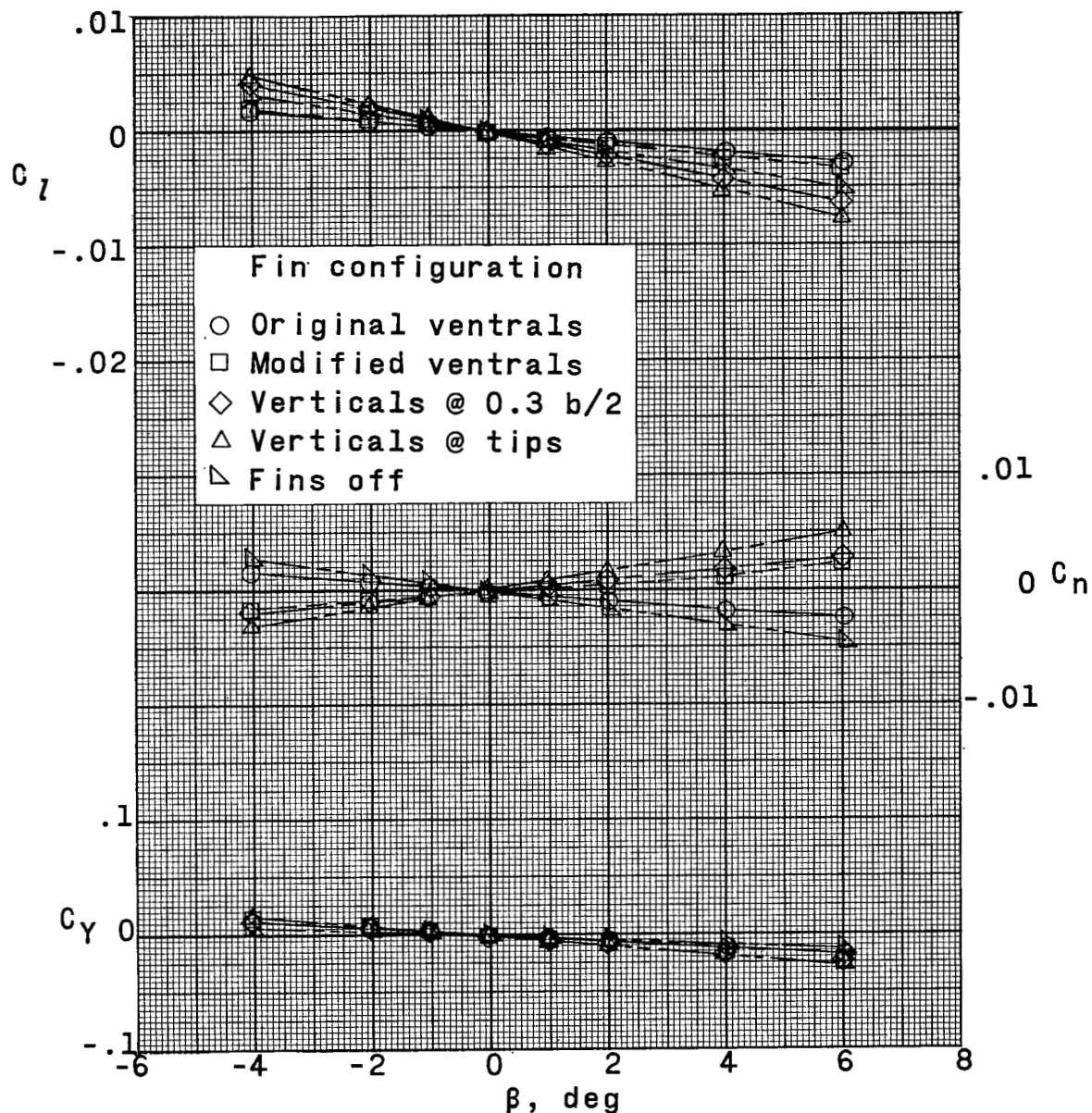
Figure 20.- Effect of ventral and vertical fins on aerodynamic character-
istics in sideslip. Modified forebody at 2.9°; δ_c = 2.9°; M = 3.00.

(b) $\alpha \approx 4^{\circ}$.

Figure 20.- Continued.

(c) $\alpha \approx 10^{\circ}$.

Figure 20.- Concluded.

Fin configuration

○ Original ventrals
□ Modified ventrals
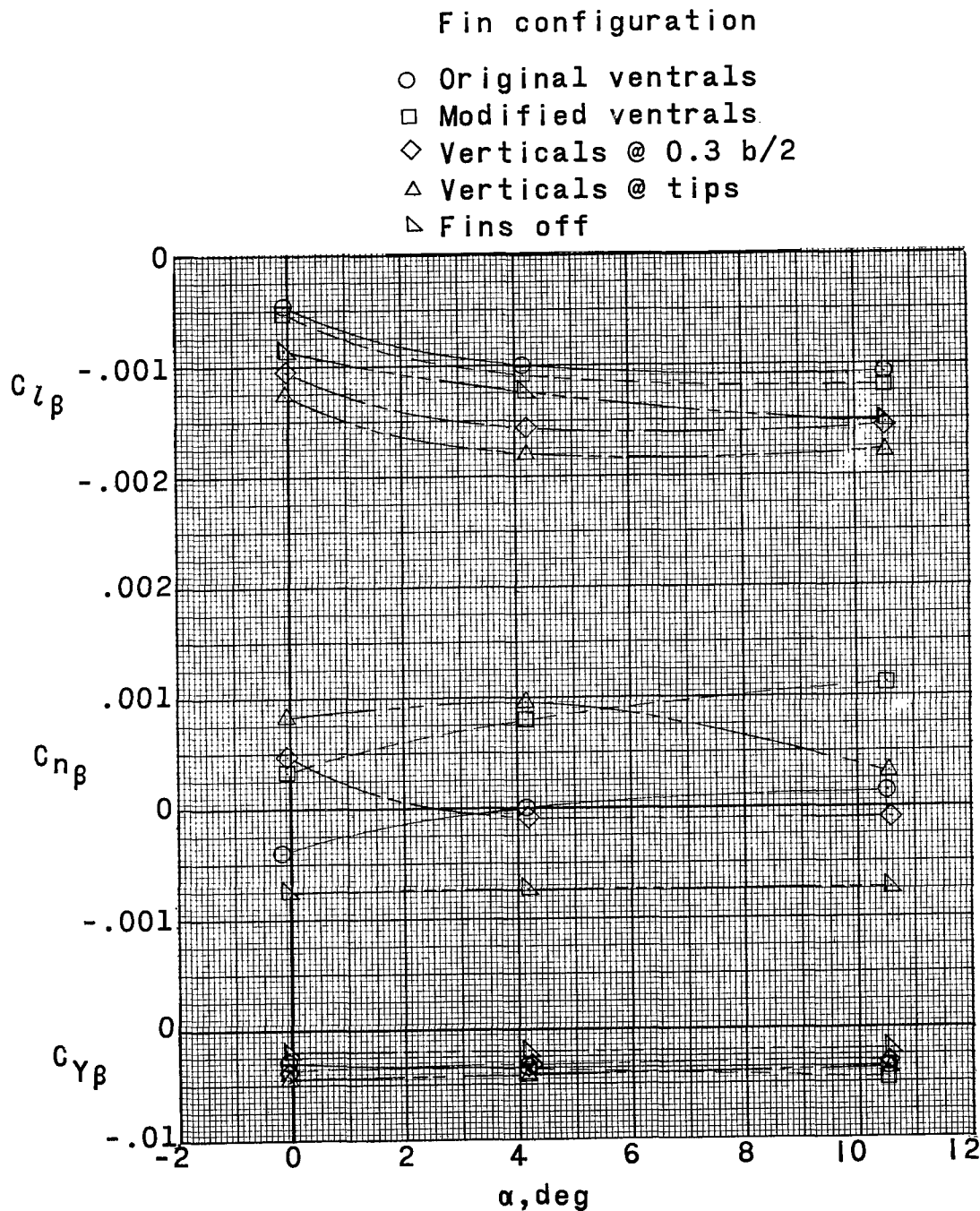◇ Verticals @ 0.3 b/2
△ Verticals @ tips
◁ Fins off

Figure 21.- Effect of ventral and vertical fins on the static lateral and
   directional stability derivatives with angle of attack. δ_c = 2.9°;
   M = 3.00.